Experimental Investigation of Rotorcraft Outwash in Ground Effect

Philip E. Tanner and Austin D. Overmeyer
U.S. Army Joint Research Program Office, Aeroflightdynamics Directorate
NASA Langley Research Center, Hampton, VA 23681

Luther N. Jenkins and Chung-Sheng Yao
Flow Physics and Controls Branch
NASA Langley Research Center, Hampton, VA 23681

Scott M. Bartram
Advanced Measurement and Data Systems Branch
NASA Langley Research Center, Hampton, VA 23681

Abstract

The wake characteristics of a rotorcraft are affected by the proximity of a rotor to the ground surface, especially during hover. Ground effect is encountered when the rotor disk is within a distance of a few rotor radii above the ground surface and results in an increase in thrust for a given power relative to that same power condition with the rotor out of ground effect. Although this phenomenon has been highly documented and observed since the beginning of the helicopter age, there is still a relatively little amount of flowfield data existing to help understand its features. Joint Army and NASA testing was conducted at NASA Langley Research Center using a powered rotorcraft model in hover at various rotor heights and thrust conditions in order to contribute to the complete outwash data set. The measured data included outwash velocities and directions, rotor loads, fuselage loads, and ground pressures. The researchers observed a linear relationship between rotor height and percent download on the fuselage, peak mean outwash velocities occurring at radial stations between 1.7 and 1.8 *r/R* regardless of rotor height, and the measurement azimuthal dependence of the outwash profile for a model incorporating a fuselage. Comparisons to phase-locked PIV data showed similar contours but a more contracted wake boundary for the PIV data. This paper describes the test setup and presents some of the averaged results.

Nomenclature

A	rotor disk area, ft^2
C_P	rotor power coefficient, $P/\rho A\Omega^3R^3$
C_T	rotor thrust coefficient, $T/\rho A\Omega^2R^2$
C_T/σ	blade loading coefficient
DL	disk loading, lb/ft^2
GRMS	General Rotor Model System
h	measurement vertical location, ft
IGE	in ground effect
LaRC	Langley Research Center
OGE	out of ground effect
P	rotor power, hp
p	ground static pressure, lb/ft^2
PIV	Particle Image Velocimetry
R	rotor radius, ft
r	measurement radial location, ft
RTC	Rotor Test Cell
T	rotor thrust, lb
T_∞	rotor thrust OGE, lb
V_h	hover induced velocity, $\Omega R\sqrt{C_T/2}$, ft/s
V_r	radial outwash velocity, ft/s
z	rotor hub height, ft
ρ	air density, slug/ft^3
φ	roll angle, deg
Ψ	measurement plane azimuth angle, deg
Ω	rotor rotational speed, rad/s

Presented at the AHS 71st Annual Forum, Virginia Beach, Virginia, May 5–7, 2015. AMRDEC Public Release Control Number PR1615.

Introduction

The behavior of the wake of a rotorcraft can be greatly influenced by the proximity of the rotor to obstacles that disturb the development of the rotor wake or constrain the flow into the rotor. The most significant of these obstructions is the ground surface. In Ref. 1, Leishman states that while the effect commonly referred to as ground effect has been observed since the dawn of the helicopter age, the aerodynamics governing the rotor wake under these conditions are still not fully understood. This phenomenon most prominently affects rotorcraft operating in hover, but it also

influences performance during low speed forward flight. For rotorcraft hovering close to the ground, the rotor slipstream must rapidly expand as it approaches the surface, transitioning from the mostly-vertical downwash to radial outwash that develops into a radial wall jet (Ref. 2). This alters the velocity of the slipstream and the induced velocity, which in turn affects the rotor thrust and power. A comparison of wake behaviors is illustrated in Figure 1. The image on the left (a) shows a rotor hovering out of ground effect (OGE), where the rotor wake behaves without effect from any outside disturbance and displays the natural contraction to the far wake region, while the right image (b) depicts a rotor hovering at an altitude approximately 2 rotor radii high, and thus in ground effect (IGE), and the rotor wake that results.

Much work has been done in the past to investigate the behavior of the rotor wake in and out of ground effect. Experiments using models with a variety of rotor sizes have been conducted, ranging on the order of a few inches in radius (both isolated, Ref. 3, and with a fuselage, Ref. 4), to more common model rotor radius sizes of one to five feet (e.g., Refs. 6-8), to very large rotors, such as a 37.5 ft (Ref. 9) or 46 ft (Ref. 10) radius. Most of these past tests did not investigate the effect that the fuselage had on the behavior of the wake as they were either performed using an isolated rotor or did not have the capability of removing the decreased fuselage download from the measured reduction in thrust required as the rotor height was lessened. Flight tests have been performed using a number of military and civilian airframes to better understand the performance effects of operating a rotor close to the ground. Many of these flight tests also measured the resulting radial outwash velocities close to the ground, helping to define the operational environment and develop safe working zones for personnel conducting operations on the ground nearby. Most of these measurements were obtained using traversing arrays of pitot probes (Ref. 11), mechanical anemometers (Refs. 12 and 13) or ultrasonic anemometers (Refs. 14-16).

There have been several studies that examine the effect of impinging jets onto a ground surface, and while geared more towards VTOL aircraft with extremely high disc loadings, they still display the outwash characteristics and the associated wall jet similar to rotorcraft. These are notable in that many of the studies observed turbulent fluctuations propagating radially from the impingement region (Ref. 17) with an almost periodic nature at times (Ref. 18). This periodicity was discovered to be caused by the formation, coalescence and breakdown of roll-up ring vortices (Ref. 19). Also observed was the existence of stagnation bubbles in the impingement region (Ref. 20) and even movement/oscillation of the impingement point, occasionally stretching and transitioning into an impingement line (Ref. 19).

In the most ideal case, operating a rotorcraft within the ground effect region results in an increase in measured thrust for a given power when compared to that same power condition out of ground effect (or, conversely, a reduction in the power required for a given thrust). This thrust augmentation increases in magnitude as the rotor height above the ground surface is reduced. Figure 2, which builds on Johnson's work in Ref. 21, shows the ratio of thrust required at a specific rotor height IGE to the corresponding OGE thrust value, plotted against the rotor height (which is non-dimensionalized by the rotor radius). The experimental data is taken from a variety of flight test and model test sources with extensively different rotor sizes (Refs. 5-7 and 22-29) and includes data from this test effort (referred to as test number T613). Also plotted are curves based on empirical models developed by Cheeseman and Bennett (Ref. 25), Hayden (Ref. 30), Law (Ref. 31) and Zbrozek (Ref. 24). This figure shows that there is a significant thrust augmentation in hover due to the presence of the ground surface for rotor heights around two radii (one diameter) and less. Also evident is that the rotor is generally considered to be fully OGE at rotor heights of at least three rotor radii, although some researchers prefer to define OGE as rotor heights above four radii. In Harris' book on helicopter performance and design (Ref. 32), he comments that very few conventional helicopters can experience a rotor height ratio less than 60% of the radius based on the physical dimensions of the aircraft, as the rotor hub is generally at a height of at least this magnitude when the aircraft is on the ground and not in flight. The IGE behavior can be complicated by the angle of the ground surface beneath the aircraft, the presence of obstacles in the flowfield, the environmental conditions and the flight dynamics during the approach to hover. Leishman notes in Ref. 1 that observations suggest the magnitude of the effects caused by the presence of the ground plane are influenced to varying degrees by a number of rotor parameters such as the blade loading, aspect ratio, solidity, and blade twist and tip shape. Ground effect can also impact tail rotor performance a measurable amount (Ref. 32). Some of the existing empirical models attempt to address the effects of these variables.

Operationally, the resulting reduction in the power required for a given thrust condition allows a helicopter to hover IGE at a higher gross weight or density altitude

than would be possible under the same conditions OGE. It also serves as a sort of cushion that is felt near the ground when a helicopter is descending to land (Ref. 1). These benefits, however, can lead to overloading aircraft such that they can hover initially after takeoff but fail to gain altitude once they attempt to ascend outside of the IGE region. It should be noted that this effect is different from power settling, in which an increase in power is required during a descent in order to overcome the losses encountered by the wake behavior being unable to convect away from the rotor (Ref. 1). Another aspect of IGE and OGE hover that has been explored very little is the effect that obstacle-induced and wind-induced recirculation has on rotor performance. The obstacle-induced recirculation aspect is particularly important for rotorcraft operating in urban environments, not only for military operators, but also for civilian operators flying in air ambulance and business roles.

While there have been a number of computational models developed to predict the IGE wake behavior for both hover and low speed forward flight using vortex methods and grid-based computational fluid dynamics, there has been relatively little success in accurately predicting the rotor performance when compared to experimental results, especially in hover (Ref. 1). Industry in general tends to optimistically predict the hover performance of new aircraft, with the actual (reduced) hover capability only realized during flight testing (Ref. 32). Observations by personnel operating close to a rotorcraft hovering IGE note an unsteady, pulsating nature of the resulting outwash and radial wall jet that is not at a steady *n*-per-rev frequency, yet there is little experimental data that demonstrates this, limiting its adaptation into prediction codes. Also, while multiple data sets exist for both full scale and model scale tests, they generally lack the broad parameterization that is crucial to understanding the effects that individual rotor parameters have on the rotor wake characteristics.

The prediction models are used for a number of tasks throughout the evolutionary stages of design of a rotorcraft. In the initial design stage, a full parametric model could be used to predict the rotor performance of a design throughout the entire flight regime, both IGE and OGE, based on a number of design inputs. Accurate prediction models are necessary to determine, in the absence of flight testing, if and where safe operating locations exist for personnel working underneath the aircraft during low-altitude hover. As some of the designs of the aircraft that are part of the Army's Future Vertical Lift program exhibit relatively high disc loadings, these predictions are crucial in determining if sufficiently-sized areas of safe operations would exist for personnel operating and obstacles located nearby the conceptual aircraft. Similar downwash and outwash models can also be used for brownout cloud prediction methods in order to improve the understanding of the degraded visual environment that results from the large dust clouds caused by helicopter operations close to the ground of an unimproved landing site. In this scenario, the high radial flow velocities near the ground can lift up loose surface particles, evolving into large dust clouds (or snow clouds if in an arctic environment) that can obscure a pilot's vision and cause spatial disorientation that can potentially lead to loss of the aircraft and/or passengers (Ref. 33). These brownout prediction models depend on an accurate representation of the rotor flowfield and wake characteristics throughout the OGE and IGE regions in order to reasonably predict the key features of the resulting cloud, such as its size, shape, and growth rate.

Test Description

Joint U.S. Army and NASA testing was conducted at NASA Langley Research Center (LaRC) in order to address the knowledge deficiency that exists regarding rotor outwash IGE. The data presented in this paper were gathered during the first and second phases of a broader test effort that is planned to occur over multiple test entries. The first phase was test number T589 and took place in 2011, and the second entry was test number T613 and occurred in 2014. Both tests were performed using a model of a generic transport fuselage coupled with a rotor that was relatively large compared to the majority of historical downwash/outwash tests that have been conducted using a rotor model. A number of different experimental measurement techniques were performed throughout the duration of the tests, primarily in an effort to quantify the outwash velocities at various heights and radial locations around the ground plane for different hover conditions. Also measured were pressures on the ground plane and fuselage download values. While some data from T589 will be included, the focus of this paper will be the outwash results obtained during T613.

Description of the Model

The testing was conducted in NASA LaRC's Rotor Test Cell (RTC), a large chamber measuring 40 ft wide, 68 ft long and 43 ft tall that is part of the 14- by 22-Foot Subsonic Tunnel facility. The test used the Army's General Rotor Model System (GRMS), a rotor drive system that is able to be fully contained within a fuselage. As described by Murrill (Ref. 34), the system

uses two 75 hp (55.9 kW) water-cooled electric motors capable of driving a rotor with a diameter up to 13.1 ft. By design, the GRMS dynamically decouples the model support hardware from the rotor drive system through the use of pitch and roll spring-damper systems, which lowers the possibility of encountering ground resonance during testing. Two internal six-component strain gauge force and moment balances enable the independent measurement of rotor and fuselage aerodynamic loads, a measurement that cannot be made during flight testing. Specifically, NASA's MK XXXA balance was used to measure rotor loads during both tests, while the 748 and 1630B balances were used to measure the fuselage loads during T589 and T613, respectively. The balance specifications are given in Table 1.

The GRMS was installed using a sting-mounted configuration, employing a dogleg adapter that was enclosed in the fuselage to attach to a long support sting. The sting was mounted in a cantilevered manner to the movable mast installed in a facility model cart. The distance from the center of the mast to the rotor hub center was approximately 29 ft (5.25*R*). The model cart was powered such that the vertical mast supporting the sting could raise, lower and pitch, permitting non-dimensional rotor height values between 0.872 and 2.093 *z/R* to be achieved while holding the rotor disk parallel to the surface. During T613, the sting included a roll adapter that enabled the entire model to roll and was the first time in this facility that a rotorcraft model had been used in conjunction with this adapter. Given that this was a new setup, extensive forced vibration testing was performed prior to the rotor testing to ensure ground resonance frequencies would be avoided.

A four-bladed fully articulated hub with a 5.54 ft rotor radius (*R*) was used for this test. The rotor was operated at 1150 RPM, giving a tip velocity of 667 ft/s (Mach 0.58), similar to that of a full scale rotorcraft. The blades possessed -14° of linear twist and represented an advanced, modern rotor using RC-series airfoils. Additional details on the rotor can be found in Refs. 35 and 36. The fuselage shell was the NASA ROBIN-Mod7 fuselage, an analytically-defined helicopter fuselage model that has been used in numerous prior tests and is meant to represent a generic transport aircraft. Greater detail of the fuselage geometry can be found in the publications by Schaeffler et al. (Refs. 37 and 38).

A second model cart centered laterally under the model rotor hub was utilized as the ground plane. Longitudinally, the rotor hub was located closer towards the rear edge in order to align the blade at an azimuth of 270° with a window inset in the cart used for obtaining pressure sensitive paint measurements on the blade. The cart had a surface measuring approximately 20.0 ft (3.61*R*) long and 21.33 ft (3.85*R*) wide, and the lengthwise distance between the center of the rotor and the front edge (at the 180° azimuth) was 10.75 ft (1.94*R*). A diagram of the test setup in the RTC is presented in Figure 3, while Figure 4 shows an image of the test setup with the model at a rotor height of 1.14 *z/R*.

Description of the Testing

A joint NASA and U.S. Army test group worked collectively throughout the duration of the tests in order to complete the test objectives. The first entry, T589, involved Particle Image Velocimetry (PIV) and pressure sensitive paint measurements as well as fluorescent oil flow visualization on the ground plane. The majority of T613 involved the measurement of the rotor outwash velocity profile using a rake consisting of nine multi-hole pitot-static probes mounted in an aerodynamic fairing and installed on a remotely-operated traverse. A photograph of this technique is provided in Figure 5. The probes were conventional, straight, seven-hole probes and were calibrated by the manufacturer. Per the manufacturer's specifications, the average angular accuracy is less than one degree, the average velocity accuracy is ±3.28 ft/s, and the probes have a 70° cone of acceptance from the probe tip. The nine instruments were distributed vertically along the rake and were more finely spaced along the lower half of the rake where it was expected that the maximum flow velocities would occur. Actual probe locations were at vertical heights (*h*) of 0.042, 0.094, 0.26, 0.43, 0.59, 0.76, 1.09, 1.43, and 1.93 ft, or non-dimensionalized using the rotor radius (*h/R*), at heights of 0.0075, 0.017, 0.047, 0.077, 0.107, 0.137, 0.197, 0.258, and 0.348. Each of the seven ports on the probes were plumbed to miniature piezoresistive unsteady pressure transducers to enable dynamic measurement capability so that unsteady flow behaviors in the outwash and well jet region could be measured along with the means. An unsteady calibration was used to quantify the effect that the short section of tubing had on the transducer frequency response.

A row of piezoresistive unsteady pressure transducers were installed in the surface of the ground plane to record static and dynamic ground pressures along the surface. These were installed along the 270° azimuthal (ψ) line every 0.25 *r/R*, with a total of eight transducers installed from 0 *r/R* to 1.75 *r/R*. These locations are shown in Figure 3 as the blue circles.

A variety of traverse survey schedules were used for the different traverse azimuth locations, rotor heights and thrust conditions. Thrust was held with an average standard deviation of 0.61% of the target thrust value, while the rotor height was held with an average standard deviation of 0.07% of the target. Four total thrust conditions were utilized throughout the test, although not all thrust and rotor height combinations were tested. A summary of the thrust coefficients (C_T) used during this testing and the respective values of the blade loading coefficient (C_T/σ) and the rotor disk loading (*DL*) is shown in Table 2. The test matrix for T613 is given in Table 3, while Table 4 gives the specifics for the different traverse survey schedules. Initially, the measurements were taken at radial locations from 0 (directly under the rotor center) out to 1.6 *r/R*, generally with 0.1 *r/R* spacing (Schedule *A*). Measurements at 0 and 0.25 *r/R* were not taken for the lowest rotor height due to clearance issues underneath the fuselage (Schedule *B*), and some runs at 270° azimuth stopped at an *r/R* of 1.5 before it was determined that the traverse could safely go to 1.6 (Schedule *C*). Some higher resolution runs were performed taking measurements at more radial stations, with Schedule *D* taking data every 0.05 *r/R* from 0.5 to 1.6 *r/R*, while Schedules *E* and *F* (for the lowest hover height) were more resolved only from 0.7 to 1.3 *r/R*, which was generally where the highest velocities and forces were observed. A few variations of Schedule *D* were performed with the probe rake raised a small margin (1 to 2.9 in) and/or inverted (resulting in the more refined probe region being located on the top half of the rake) in order to investigate the outwash region for one specific thrust and rotor height condition more thoroughly. Although measurements were taken directly underneath the rotor disk with the probe rake, these will not be presented as the flow vectors at radial stations less than 1.0*R* were likely outside of the 70° cone of acceptance of the probes and thus not an accurate representation of the flow for those locations.

A ground plane extension was added to the front of the cart (ψ = 180°) midway through T613 in order to measure the outwash at a radial location farther out than 1.6 *r/R*, a location at which the wall jet is still developing. This extension allowed the rotor outwash to develop out to a radial location of approximately 2.66 *r/R*, and is shown in the diagram in Figure 3. A photograph showing the extension can be seen in Figure 6, with the extension identifiable as the lighter part of the ground plane (prior to being painted) in front of the model. Using this cart extension, Schedules *G* and *H* were able to take measurements out to 2.6 *r/R* with the former starting at 1.0 *r/R* and taking data with a spacing of around 0.1 *r/R*, and the latter starting at 1.25 *r/R* and taking data with a spacing of 0.05 *r/R*. According to Bradshaw's work with an impinging jet (Ref. 17), the wall jet is typically not fully developed until a radial station of 3.2*R* (referenced against the radius of the jet at impingement and not at its virtual origin) with only slight changes in the velocity profile beyond that distance.

Results and Discussion

The recorded data included the outwash velocities and directions (during T613) as well as balance data, fuselage static pressures, motor parameters, rotor parameters, operating temperatures, and a number of other key values. The outwash velocity profile data were obtained from a total of 75 individual runs and over 1300 static and dynamic data points during T613. The static data points are the mean values taken from a thirty second record, during which the rotor underwent 575 revolutions. While dynamic outwash data was obtained, it will not be presented in this paper, and the focus is on the mean data obtained during T613.

Thrust Augmentation

The thrust augmentation gained from operating a rotorcraft within ground effect has historically been shown by plotting the thrust (*T*) normalized by the OGE thrust value (T_∞) versus rotor height. This also helps to determine the boundary between IGE and OGE, which has generally been accepted as being between three and four rotor radii from the ground surface to the rotor hub.

Figure 2 illustrates this thrust augmentation, presenting data from a number of model tests and flight tests (shown as the various symbols, from Refs. 5-7 and 22-29) and empirical models based on experimental data (solid lines, from Refs. 24-25 and 30-31). The orange diamonds indicate the results from the current test effort, T613. As described earlier, ground effect causes a change in the power required for a given rotor thrust with a change in rotor height. However, throughout the duration of this testing, C_T was matched between runs at the different rotor heights instead of the power coefficient (C_P). Thus, in order to determine the thrust augmentation at different rotor heights, a second-order polynomial fit was applied to the data at each rotor height to solve for C_T as a function of C_P. All of the curve fits have an average R^2 value of 0.9999 and were used in conjunction with the OGE data from T589 (OGE data was not obtained during T613) in order to populate the T613 points in Figure 2. Note that these points fall under all four of the prediction curves, except for some of the points at the highest rotor height. Many of the data

points are under the 1.0 limit of augmentation (especially at higher values of C_P and rotor height), which would incorrectly indicate slight performance gains due to being OGE. It is expected that this is a result of using data from T589 for the OGE values as the tests were separated by a time period of more than three years, during which some slight changes were made to the GRMS and setup.

Static Ground Pressures

Figure 7 shows the static ground pressures (p), normalized by DL, versus the non-dimensional radial measurement location (r/R) for different height ratios and thrust conditions. These are compared to historical data taken from Fradenburgh at multiple height ratios and a single thrust condition (Ref. 6) and Bolanovich at a single height ratio and thrust condition but two different measurement azimuths (Ref. 9). It is worth noting that Fradenburgh's measurements were taken using an untwisted 2-bladed rotor with a radius of 1 ft, while Bolanovich's measurements were obtained using a full scale 3-bladed rotor with a 37.5 ft radius and blade twist of -8°. Both of these rotors were isolated, although Bolanovich's large whirlstand was located directly underneath the rotor, and no indication is given as to how tightly spaced the static pressure measurements were taken.

Regardless of rotor thrust or height, the pressure ratio (p/DL) peaks at a value underneath the rotor disk between 0.6 and 0.8 r/R for the T613 data. Fradenburgh found similar peaks occurring just shy of the rotor disk edge, while Bolanovich's curves show multiple peaks underneath the disk beginning around 0.5 r/R. All measurements aside from the curve at ψ = 0° from Ref. 9 show that the pressure ratio approaches 0 at a radial station outboard of 1.75. The low thrust curves from T613 show a much larger effect of rotor height on the behavior of the curve, especially for heights of 1.79 and 2.09, than the high thrust condition.

True comparison to the results from Fradenburgh and Bolanovich is difficult to make since the hover conditions (rotor height and thrust) differ, but the most similar cases are the Fradenburgh curves at height ratios of 1.0 and 2.0 z/R and 0.007 C_T and the T613 runs at 0.006 C_T. The curves from the T613 data are similar in nature to the Fradenburgh curves, although there are some differences. The radial location of the peak static pressure ratio moves gradually outward as the rotor height ratio increases for Fradenburgh's data (from 0.8 r/R at the low height to 0.9 r/R at the highest height) but the T613 data displays the reverse trend for the low thrust condition with the peak location moving inward with an increase in rotor height. This could be due to the resolution of the measurements, as pressure taps were only installed every 0.25 r/R, and with the peaks indicated at 0.5 r/R for the case at 2.09 z/R and 0.75 r/R for the other two heights, it is likely that the true peak falls somewhere within the region between 0.5 and 0.75 r/R. For the high thrust condition, the peak remains constant at 0.75 r/R, but again is dependent on the resolution of the measurement location. Both sets of curves from the T613 data show that the peak magnitude increases with increasing height, which is again counter to what the data from Fradenburgh indicates.

Also observable in Fradenburgh's data is that for low rotor heights under 1.0 z/R, there is a region of negative pressure on the surface directly underneath the rotor hub center. Reference 6 indicates that this region is likely due to the presence of a strong vortex on the vertical centerline and that it was unknown if the presence of a fuselage or other object underneath the rotor would eliminate this trend. While the setup for T589 and T613 included a fuselage, the dimensions only permitted testing down to a rotor height of 0.872R, and the rotor heights in Ref. 6 that display this negative pressure (0.5R and 0.2R) are highly unlikely to be encountered by actual rotorcraft (Ref. 32). The T613 static pressure data was furthermore only obtained down to a height of 1.5 z/R, so all observed pressures underneath the hub center were positive.

Fuselage Download

Figure 8 shows the average fuselage percent download values versus the rotor height ratio z/R for cases from T589 and T613. At 0° pitch and roll, a positive download is acting on the fuselage opposite of the rotor lift vector. The percent download is calculated from dividing the download by the total lift, which is approximately the download subtracted from the rotor thrust. Each point on the plot represents the average from several static data points for multiple runs at each specific rotor height/thrust combination. The use of the percent download normalizes the data for small variations in C_T. The vertical error bars shown for each point indicate the maximum and minimum static readings for the respective measurement during the runs at each condition (around 15 points), and are not the maximum and minimum readings from dynamic data during a single dynamic data point. With a lower normal force range and increased accuracy for the 748 balance used in T589 versus the 1630B balance used in T613 (see Table 1), there is greater uncertainty in the download data obtained during the most recent test, evidenced by

the relative size of the error bars for the different tests, especially at the higher rotor heights.

The relatively linear relationship between rotor height and fuselage download can be observed, and the gradient is slightly less steep as the thrust is increased. Note that, as these are percent download values, the figure is not indicating that the actual download values are decreased for the increasing thrust values, but that the magnitude of the download relative to the increased lift decreases as thrust is increased. A fascinating observation is the existence of negative percent download values at the lowest rotor height for the T613 data for both thrust conditions, which indicates a total lifting force acting on the fuselage at this height. This could be due to the fountain effect that occurs from the recirculation underneath the fuselage at low hover heights, although further investigation of the flow characteristics in this region are required for certainty. Also observable are the differences between the individual tests as T589 shows marginally higher measured percent download values for the same rotor thrusts.

Mean Outwash Velocities

The primary goal of this downwash/outwash test effort during T613 was to measure the outwash velocity (V_r) profiles at different radial (r/R) and azimuthal (ψ) locations for various hover conditions. This section presents some of the mean outwash velocities that were measured and discusses the effects that different parametric changes of the model have on the outwash behavior.

Effect of Rotor Height

A comparison of the radial outwash velocity data at five different rotor heights is presented in Figure 9, with the measurements taken at an azimuth of 180° and with the ground extension in place. The velocity has been non-dimensionalized using the average hover inflow velocity V_h, calculated from momentum theory assuming a uniform inflow and the averaged rotor thrust conditions during the associated runs. Non-dimensionalizing the data this way has been done in past outwash measurement tests (e.g., Refs. 3 and 39) and enables more direct comparisons to other model tests and flight tests to be made.

Evident in these plots is that the maximum velocities in the wall jet are nearly twice the hover inflow velocities at the lowest rotor height. In Ref. 3, in which the researchers used PIV to observe the wake of a small-scale (0.282 ft radius) rotor, at a rotor height of 1.0 z/R, the maximum average outwash velocities exceeded $2V_h$ at a radial station around 1.5 r/R. Flight test data from Harris et al. on the CH-53E, obtained using multi-axis ultrasonic anemometers, also showed maximum average outwash velocities at the same conditions (rotor height of 1.0R and radial station of 1.5 r/R) around $2.1V_h$, regardless of thrust (Ref. 14). However, again using anemometers, maximum average measured outwash velocities at 1.0 z/R and 1.5 r/R were $1.9V_h$ for the HH-60H (Ref. 40) and V-22 (radially outboard parallel to the wing, Ref. 41), and around $1.7V_h$ for the CH-47D (Ref. 16).

Also observable is the high-velocity region in the wall jet, especially at the lowest rotor heights, visible as the orange pocket extending to a maximum height around 0.15 h/R at 1.5 r/R (for the 0.87 z/R case). By around 1.75 r/R, all of the velocity vectors are parallel to the ground surface for all rotor heights, and slightly more inboard as the rotor height increases. The high-velocity region in the wall jet is proportionally taller at the lower rotor heights, and by a rotor height of 2.09R, the high-velocity region has largely dissipated. Notable is the area of quiescent flow outside of the boundary of the rotor wake and its changes with rotor height. This is visible as the blue, zero radial velocity region on the top of each plot. The rotor wake is more contracted at the lower rotor heights and expands as the rotor height is increased.

The related outwash velocity profiles with velocities non-dimensionalized are shown in Figure 10, with the symbols indicating the heights at which the measurements were taken. Apparent in this figure is that the shape of the velocity profile of the wall jet varies, as inboard the profile is almost uniform vertically for all rotor heights. By 1.25 r/R, however, the profile transitions to have a high-velocity region, which is itself almost uniform, spanning to a height of 0.15R. The peak velocity gradually increases, and the maximum velocity occurs around a radial station between 1.7 and 1.8 r/R regardless of rotor height. The low rotor heights tend to have the peak velocity concentrated low to the ground at a height of about 0.02R, while the highest rotor height displays peak velocities higher up, closer to 0.08R. This is important as the vertical location of the peak force, and not solely its magnitude, affects the response of personnel operating within the vicinity of outwash (Ref. 14) as this location affects the strength of the overturning moment. The velocity trend is reversed above 0.15R for radial stations outboard of 1.25R, with the higher rotor heights having greater outwash velocities than the lower heights. Therefore, even though the forces decrease as the rotor height is increased, the ease of working within the outwash could

be more difficult at the higher rotor heights than the lower ones, depending on the resulting outwash velocity profile.

Effect of Rotor Thrust

Shown in Figure 11 is a comparison of the mean radial outwash velocities and vectors at three different rotor thrust coefficients (0.006, 0.008 and 0.009) at a constant rotor height of 1.140*R*. The velocities were again taken at an azimuth of 180° and are presented in engineering units of ft/s without being non-dimensionalized, as doing so minimizes the thrust dependency on the plotted velocities.

The direct comparison of rotor thrusts makes clear the interdependence of rotor thrust on the wall jet velocity profile. However, the thrust does not significantly affect the height or shape of the rotor wake as all three thrust conditions share a similar wake boundary shape, with the quiescent region moved slightly inboard as the thrust decreases. The thrust does affect the duration of the high-velocity area inside the wall jet. For the low thrust case, the wall jet is fully developed and has reached a constant velocity with respect to height above the surface by the final measurement location at 2.6 *r/R*. However, for the higher thrust conditions, the region with high velocities inside the wall jet continues farther out past the 2.6 *r/R* station, although the velocities in this region are decreasing.

Effect of Measurement Azimuth

A comparison of the mean radial non-dimensionalized outwash velocities and velocity vectors at different azimuthal locations is shown in Figure 12 for the rotor at 1.140*R* and at a C_T of 0.008, while Figure 13 shows the related non-dimensionalized velocity profiles at select radial stations. These measurements were taken without using the extension to the ground plane, as that would have permitted measurements at radial stations past 1.60 *r/R* only at the 180° and 210° azimuths. Examining the figures, the outwash measurements at the 180° and 210° display similar behaviors. Comparing the contours for these two azimuths, the high-velocity region in the wall jet has a distinct vertical formation at 1.25 *r/R* and height of about 0.1*R* at 1.6 *r/R*. The velocity contours fall very near to one another for all radial measurement locations.

Progressing around the rotor azimuth, the rotor wash at the four planes evaluated between 240° and 330° exhibit comparable behaviors. The start of the high-velocity region is more wedge-shaped, starting to form around 1.15 *r/R*, and also has a higher thickness at 1.6 *r/R*, extending up close to 0.15*R*. The reduced strength of the mean outwash for the azimuths extending over the nose of the model is likely due to the presence of the fuselage, as the region from 240° to 330° has roughly only the root cutout section of the rotor disk directly above the fuselage. Visible at radial stations past, and including, 1.2 *r/R*, the velocity profiles in this region tend to agree well with one another. At 1.2 *r/R*, the velocity peaks around 1.5V_h at a height of 0.2*R*, reaching a maximum velocity of 1.8V_h at 1.6 *r/R* with the height dropping to around 0.1*R*. At 360° ψ, the rotor wake boundary is much more contracted than at the other measurement azimuths. Correspondingly, the velocity profiles also show some contraction as the peak velocities are located at a lower height than for the other azimuths. This azimuth directly under the tail and sting shows a higher peak velocity, approaching 1.9V_h at the 1.6 *r/R* station and close to 0.02 *h/R*. As discussed earlier, the wall jet is still developing at 1.6 *r/R* with the maximum velocities experienced around 1.7 *r/R* (at 180° azimuth), so comparisons regarding the true peak velocity values and radial locations of these cannot be made.

This seems to concur with past results, as historical flight tests of a single main rotor airframe have indeed shown an azimuthal dependence on the outwash characteristics (e.g., Refs. 14-16), while isolated rotor tests have not investigated the change in wake with respect to the measurement azimuth. However, Donaldson et al. did observe that for an isolated jet impinging on a surface, there was a lack of any significant dependence of the azimuth on the behavior of the wall jet, which they attributed to being a result of the turbulent mixing that governs the flow (Ref. 42). The azimuthal dependence likely arises, or is at least amplified, by the presence of the fuselage in the downwash and should be investigated further either experimentally or computationally.

Effect of Model Roll Angle

Figure 14 presents the mean radial non-dimensionalized outwash velocities and velocity vectors at a constant rotor hub height of 1.140*R* and azimuth measurement location of 270° for different model roll angles (φ). Figure 15 shows the corresponding non-dimensionalized velocity profiles at select radial locations. Positive roll indicates a clockwise angle from the pilot's perspective, so at 270° azimuth the rotor tip would be higher for positive roll and lower for negative roll. For comparison purposes, results from a single case at a rotor height of 0.965*R* and 0° roll are included. This is the height at which the location of the rotor tip at 270° azimuth would be the same as that for a roll angle of -10° at rotor height

of 1.140*R* when considering the blade coning angle. Given that the measurements were taken at an azimuth of 270°, the ground plane extension was not utilized for this investigation.

At -10° roll, the rotor wash is more contracted with a wake boundary height around 0.27*R* at 1.6 *r/R*, much lower than the level case at the same rotor hub height (0.32*R*) and close to the level case at the same rotor tip height (0.29*R*). The high-velocity region of the wall jet is correspondingly moved much farther inboard and shaped differently, forming with a sharp edge around 1.05 *r/R* as opposed to having an angled edge with a formation beginning around 1.2 *r/R* for the level cases (at both 0.965 and 1.140 *z/R*). The high-velocity region is also more contracted, having a lower maximum height than the level cases. The peak average velocity is reached farther inboard as well, occurring around 1.5 *r/R* versus around 1.7 *r/R* for the level case, although the latter was at 180° azimuth (Figure 10).

Working the other direction, at positive 10° roll, the high-velocity region begins forming around 1.5 *r/R*, much farther out than for the same condition at a level hover. The observable maximum velocities at this positive roll angle are significantly lower when compared to the same condition at a level hover in the limited region of measurement. Velocities peak at approximately 1.6V_h at a radial station of 1.6 *r/R* and height of 0.12 *h/R* for the 10° rolled case versus the same values of 1.8V_h at 1.6 *r/R* and height of 0.05 *h/R* for the level case. At 270° azimuth, the rotor tip is at a height of approximately 1.3 *h/R* when taking the coning angle into account. With the linearity of the rotor wash behavior for rotor heights above 0.75*R*, one would expect the outwash behavior to fall between that for rotor heights of 1.14 and 1.5 *z/R* if rolling the model only had the effect of essentially changing the rotor height at a specific azimuth. Looking back at Figure 9 and Figure 10 (although at 180°), this would have the high-velocity region forming with a vertical edge around 1.25 *r/R* for a comparable rotor tip height.

The effect of the roll angle was also investigated at the lowest rotor height of 0.872*R*. Shown in Figure 16 are the non-dimensionalized velocity contours and associated velocity vectors at 270° ψ for different model roll angles. Again visible for the negative roll is the stronger contraction of the rotor wake, with the boundary more than 30% lower at 1.6 *r/R* when compared to the no roll case, and the movement inboard of the high-velocity region. Figure 17 shows the related velocity profiles for these three cases. While the maximum velocities for the -10° and 0° cases are similar (around 1.95V_h), the -10° case peaks earlier (at 1.5 *r/R*) and has a much shallower profile arising from the contraction. The wall jet for the 10° case is not fully developed by the last radial measurement station of 1.6 *r/R*. The rotor tip at a 270° azimuth for -10° roll, with flapping accounted for, is at a height of approximately 0.7 *h/R*. It is interesting to note that decreased wall jet velocities observed in Ref. 3 for heights below 0.75 *z/R* do not appear to apply when only part of the rotor disk is below that threshold. This investigation demonstrates that roll does not simply simulate a change in the rotor height for a given azimuthal location, but also introduces a contraction/expansion in the wall jet depending on roll direction and region of interest, leading to lower maximum velocities located more outboard for positive roll and higher maximum velocities located farther inboard for negative roll.

PIV Comparison of Mean Outwash Velocity

Particle Image Velocimetry data was obtained by researchers from LaRC's Flow Physics and Control Branch and Advanced Measurements and Data Systems Branch during T589. The data presented was taken at a rotor height of roughly 1.14*R* and average C_T of 0.008, and the region of interest was in the 270° azimuthal plane from 0.9 to 1.9 *r/R* at heights up to 0.35*R*. Data from a height of 0*R* to 0.02*R* has not been included due to flare off of the model cart affecting the results obtained close to the surface. The PIV data presented was averaged from seven sets of 100 image pairs, taken with the rotor phase locked at a rotor azimuth of 295° and using a pulse separation of 100 μs.

Figure 18 presents a comparison of the mean outwash velocities (again non-dimensionalized by V_h) obtained from PIV (shown at the top) to numerous data sets gathered using the multi-hole probe rake at similar conditions, with the first set at 270° azimuth for a direct comparison and the last two sets at 180° azimuth for comparison to a wider radial station. Figure 19 shows the mean non-dimensionalized velocity profiles at different radial locations for the PIV and probe rake data acquired at the same measurement azimuthal location. It should be noted that two artifacts appear in the PIV contour (one on the boundary of the high-velocity region at approximately 1.6 *r/R* and the other near the surface at 1.9 *r/R*) are due to the laser light being scattered off of an object in the background. This is also what causes the sharp discontinuity in the velocity profile for 1.6 *r/R* around a height of 0.14*R* in Figure 19. While the measurements taken using the different techniques show similar features and overall behavior, there are some dissimilarities that appear, These should

be expected given that the PIV data was obtained with the rotor phase locked, whereas the probe rake data was averaged over all rotor azimuths during 575 rotor revolutions.

Comparing the PIV data to the probe rake data at 270°, the PIV phase-locked data show a much more contracted wake boundary and an earlier formation of the high-velocity region. At 1.6 *r/R*, the farthest outboard measurement obtained using the probe rake at 270°, the rotor wake boundary exists around 0.3*R* high, whereas the PIV displays the same boundary at 0.24*R*. PIV shows the formation of the high-velocity region occurring more inboard, with velocities around 1.5V_h beginning near 1.1 *r/R* 0.2*R* high, while these velocities appear about 1.25 *r/R* for the probe rake data. The maximum velocities in the PIV data appear to be higher for the same radial station when compared to the mean probe rake data, with velocities approaching 1.95V_h, while the probe rake data show maximum velocities around 1.8V_h. The height location of the peak velocity varies, as the greater contraction shown by the PIV data causes the peak velocity to occur at a lower height.

A direct comparison of the PIV data at 270° azimuth to the probe rake data at 180° is more difficult to make. As was noted previously, there appears to be an azimuthal dependence on the rotor wake due to fuselage interference, so it should be expected that the PIV data from 270° would exhibit features that are slightly different than those for velocity measurements taken at 180° in addition to the differences already described. The PIV data shows that the high-velocity region at 1.9 *r/R* is approximately 50% of the total wall jet thickness, while both cases from the probe rake data at 180° azimuth show a proportionally shallower high-velocity region at the same radial station, which is about 30% of the total thickness.

Summary and Conclusions

A comprehensive characterization of the outwash of a model scale rotorcraft in hover was conducted during joint U.S. Army and NASA testing at NASA LaRC's 14- by 22-Foot Subsonic Facility's RTC over the course of two entries that are part of a broader test effort. Velocity profiles were measured at various azimuthal and radial locations with the model at different heights, thrust conditions, and roll angles and included both mean and dynamic data, while only the mean data is presented in this paper. Other key operating parameters and measurements such as rotor and fuselage aerodynamic loads and ground static pressures were recorded as well. The following can be concluded from this work:

1. Static ground pressures were obtained for the three highest rotor heights and showed static pressure peaks underneath the rotor disk between 0.6 and 0.8 *r/R*, agreeing with past measurements by Fradenburgh under similar conditions (Ref. 6).
2. Fuselage download measurements from T589 and T613 indicated a linear relationship between rotor height and fuselage download for both the high and low thrust cases. At the lowest rotor height and regardless of thrust, there is a total lifting force acting on the fuselage, possibly as a result of the fountain effect in the recirculation region, although more detailed flow measurements are required to be certain.
3. The expected dependence of the outwash wall jet velocity from the rotor height was observed. The formation location of the high-velocity region in the wall jet moved farther outboard as rotor height increased. Peak mean velocities occurred at radial stations between 1.7 and 1.8 *r/R*. At radial stations 1.5 *r/R* and outboard, all rotor heights have matching outwash velocities approximately 0.15*R* high. Maximum non-dimensionalized velocities with respect to V_h approach 2.0.
4. Thrust does not appear to affect the location of the IGE rotor far wake boundary, unlike rotor height, but does affect the extent of the high-velocity region inside the wall jet.
5. Comparison of outwash profiles taken at different azimuthal locations showed that, while similar in nature, there was an observable difference in mean profiles for azimuthal locations extending over the fuselage compared to those extending from the side of the model. Given that past tests have shown a lack of azimuthal dependence for isolated rotors and impinging jets, this is likely due to the presence of the fuselage.
6. Rolling the model changed the shape of the high-velocity formation region and depending on roll direction either contracted or expanded the rotor wake boundary. The roll investigation showed that rolling did not simply simulate a change in rotor hub height for a given rotor azimuthal location.
7. Comparisons to PIV data acquired during T589 were made and indicate some differences in the rotor wake shape and wall jet velocity profile. The phase-locked wake boundary is much more contracted for the PIV measurements and displays a higher-velocity wall jet for the same radial station.

Acknowledgements

The authors would like to thank the members of AFDD JRPO for their guidance and support throughout the duration of this test effort and publication. Also, this work would not have been possible were it not for the professional staff of NASA's 14x22 tunnel to aid in experimental set up, rotor maintenance, test operations, and data acquisition and reduction.

References

[1] Leishman, J.G., *Principles of Helicopter Aerodynamics, 2nd Edition*, Cambridge University Press, New York, New York, March 2006, pp. 257-262.

[2] Glauert, M.B., "The Wall Jet," *Journal of Fluid Mechanics*, Vol. 1, Iss. 6, December 1956, pp. 625-643.

[3] Lee, T.E., Leishman, J.G., and Ramasamy, M., "Fluid Dynamics of Interacting Blade Tip Vortices with a Ground Plane," American Helicopter Society 64th Annual Forum, 29 April-1 May, 2008.

[4] Sydney, A., and Leishman, J.G., "Measurements of Rotor/Airframe Interactions in Ground Effect Over a Sediment Bed," American Helicopter Society 69th Annual Forum, Phoenix, Arizona, 21-23 May 2013.

[5] Koo, J., and Oka, T., "Experimental Study on the Ground Effect of a Model Helicopter Rotor in Hovering," Translation of National Aerospace Laboratory Report NAL-TR-113, Tokyo, August 1966, NASA Technical Translation TT F-13938, December 1971.

[6] Fradenburgh, E.A., "Aerodynamic Factors Influencing Overall Hover Performance," Advisory Group for Aerospace Research and Development Conference on Aerodynamics of Rotary Wings, Proceedings No. AGARD-CP-111, September 1972, pp. 7-1 to 7-11.

[7] Light, J.S., "Tip Vortex Geometry of a Hovering Helicopter Rotor in Ground Effect," American Helicopter Society 45th Annual Forum, Boston, Massachusetts, 22-24 May 1989.

[8] Ramasamay, M., Gold, N.P., and Bhagwat, M.J., "Rotor Hover Performance and Flowfield Measurements with Untwisted and Highly-Twisted Blades," 36th European Rotorcraft Forum, Paris, France, 7-9 September 2010.

[9] Bolanovich, M., and Marks, M.D., "Experimental Downwash Velocity, Static Pressure, and Temperature Distributions in Ground Effect for a 75-Foot Jet-Driven Rotor," *Journal of the American Helicopter Society*, Vol. 4, No. 2, 1 April 1959.

[10] Harris, D.J., and Simpson, R.D., "Final Report: Downwash Evaluation under the U. S. Army Heavy Lift Helicopter Rotor," Naval Air Test Center Technical Report No. SY-17R-76, March 1976.

[11] O'Bryan, T.C., "An Investigation of the Effect of Downwash from a VTOL Aircraft and a Helicopter in the Ground Environment," NASA Technical Note D-977, October 1961.

[12] Stephenson, J.H., "Comparative Downwash and Simulated Forest Rescue Tests of the HH-3E, HH-53B and the XC-142A Aircraft," Air Force Avionics Laboratory Technical Report AFLC-WPAFB-FEB 68 145, December 1967.

[13] Patton, W.G., and Simpson, R.D., "Investigation of SH-3/HH-3 Helicopter Downwash Environment; First Report (Final)," Naval Air Test Center Technical Report No. ST-197R-71, September 1971.

[14] Harris, D.J., and Simpson, R.D., "Final Report: CH-53E Helicopter Downwash Evaluation," Naval Air Test Center Technical Report No. SY-89R-78, August 1978.

[15] Polsky, S., and Wilkinson, C.H., "A Computational Study of Outwash for a Helicopter Operating Near a Vertical Face with Comparison to Experimental Data," AIAA Modeling and Simulation Technologies Conference, Paper No. AIAA-2009-5684, Chicago, Illinois, 10-13 August 2009.

[16] Silva, M.J., "CH-47D Tandem Rotor Outwash Survey," Naval Air Warfare Center Aircraft Division Technical Report No. NAWCADPAX/EDR-2010/120, 23 September 2010.

[17] Bradshaw, B.A., and Love, E.M., "The Normal Impingement of a Circular Air Jet on a Flat Surface," Aeronautical Research Council, Reports and Memoranda No. 3205, September 1959.

[18] Ho, C. and Nosseir, N.S., "Dynamics of an Impinging Jet, Part 1: The Feedback Phenomenon," *Journal of Fluid Mechanics*, Vol. 105, 1981, pp. 119-142.

[19] Hadziabdic, M., and Hanjalic, K., "Vortical Structures and Heat Transfer in a Round Impinging Jet," *Journal of Fluid Mechanics*, Vol. 596, 2008, pp. 221-260.

[20] Rubel, A., "Inviscid Axisymmetric Jet Impingement with Recirculating Stagnation Regions," *AIAA Journal*, Vol. 21, No. 3, March 1983, pp. 351-357.

[21] Johnson, W., "NDARC: NASA Design and Analysis of Rotorcraft," NASA Technical Publication No. NASA/TP-2009-215402, December 2009, pp. 87-89.

[22] Knight, M., Hefner, R. A., "Analysis of Ground Effect on the Lighting Airscrew," NACA TR 835. Washington, D.C., December 1941.

[23] Schoppe, G., "Standschubprüfungen mit der Modell-Hubschraube und Vorversuche mit der Modell-Hubschraube (Static Thrust Tests of the

Model Helicopter Rotor and Preliminary Research of the Model Helicopter Rotor)" Forschungsbericht FB275/1, Zentrale für Technisch-wissen-schaftliches Berichtswesen über Luftfahrtforschung, translated by J. Vanier, NACA, US AMC Report No. F-TS-1003-RE, 10 September 1946.

[24] Zbrozek, J., "Ground Effect on the Lifting Rotor," Ministry of Supply Royal Aircraft Establishment, Technical Note No. Aero 1903, July 1947.

[25] Cheeseman, I.C., Bennett, W.E., "The Effect of the Ground on a Helicopter Rotor in Forward Flight," Ministry of Supply, Aeronautical Research Council Reports and Memoranda No. 3021, September 1955.

[26] George, M., Kisielowski, E., and Douglas, D.S., "Investigation of the Downwash Environment Generated by V/STOL Aircraft Operating in Ground Effeect," US Army Aviation Materiel Laboratories, Fort Eustis, Virginia, USAAVLABS Technical Report 68-52, July 1968.

[27] Rabbott, J.P., Jr., "Model vs. Full Scale Rotor Testing," CAL/AVLABS Symposium on Aerodynamics of Rotary Wing and V/STOL Aircraft, Buffalo, New York, 18-20 June 1969.

[28] Landgrebe, A.J., "An Analytical and Experimental Investigation of Helicopter Rotor Hover Performance and Wake Geometry Characteristics," US Army Air Mobility Research and Development Laboratory, USAAMRDL Technical Report No. 71-24, June 1971.

[29] Lewis II, R.B., "Army Helicopter Performance Trends," Journal of the American Helicopter Society, Vol. 17, No. 2, 1 April 1972, pp. 15-23.

[30] Hayden, J.S., "The Effect of the Ground on Helicopter Hovering Power Required," American Helicopter Society 32nd Annual Forum, Washington, D.C., 10-12 May 1976.

[31] Law, H.Y.H., "Two Methods of Prediction of Hovering Performance," USAAVSCOM TR 72-4, February 1972.

[32] Harris, F.D., "Introduction to Autogyros, Helicopters, and Other V/STOL Aircraft, Volume II: Helicopters," NASA Special Publication No. NASA/SP-2012-215959 Vol. II, October 2012, pp. 142-145, 201.

[33] Tanner, P., "Photogrammetric Characterization of a Brownout Cloud," American Helicopter Society 67th Annual Forum, Virginia Beach, Virginia, 3-5 May 2011.

[34] Murrill, R.J, "Operation and Maintenance Manual for the General Rotor Model System", SER-50986, NAS1-12674, May 1977.

[35] Noonan, K.W., "Aerodynamic Characteristics of Two Rotorcraft Airfoils Designed for Application to the Inboard Region of a Main Rotor Blade," NASA-TP-3009, AVSCOM-TR-90-B-005, 1990.

[36] Noonan, K.W., "Aerodynamic Characteristics of a Rotorcraft Airfoil Designed for the Tip Region of a Main Rotor Blade," NASA-TM-4264, AVSCOM-TR-91-B-003, 1991.

[37] Schaeffler, N.W., Allan, B.G., Lienard, C., and Le Pape, A., "Progress Towards Fuselage Drag Reduction via Active Flow Control: A Combined CFD and Experimental Effort," 36th European Rotorcraft Forum, Paris, France, 7-9 September 2010.

[38] Schaeffler, N.W., Allan, B.G., Wong, O.D., and Tanner, P.E., "Experimental Investigation of Active Aerodynamic Load Reduction on a Rotorcraft Fuselage with Rotor Effects," 32nd AIAA Applied Aerodynamics Conference, Atlanta, GA, 16-20 June 2014.

[39] Tanabe, Y., Saito, S., Ooyama, N., and Hiraoka, K., "Investigation of the Downwash Induced by Rotary Wings in Ground Effect," *International Journal of Aeronautical and Space Sciences*, Vol. 10, No., 1, May 2009, pp. 20-29.

[40] Meyerhoff, C., Lake, R., and Peters, D., "H-60 Helicopter Rotor Downwash Wind Velocity Evaluation," Naval Air Warfare Center Aircraft Division Technical Report No. SY-3R-94, 8 February 1994.

[41] Lake, R.E., Clark, W.J., and Vachalek, J.R., "V-22 Rotor Downwash Survey," Naval Air Warfare Center Aircraft Division Technical Report No. NAWCADPAX-98-88-RTR, 9 July 1998.

[42] Donaldson, C.D., and Snedeker, R.S., "A Study of Free Jet Impingement, Part 1: Mean Properties of Free and Impinging Jets," *Journal of Fluid Mechanics*, Vol. 45, 1971, pp. 281-319.

Appendix: Tables and Figures

Table 1. Fuselage and rotor balance specifications.

	Rotor	Fuselage	
	MK XXXA	748 (T589)	1630B (T613)
Normal Force (lb)	1,500	1,800	3,000
Side Force (lb)	750	1,000	1,800
Axial Force (lb)	600	500	800
Rolling Moment (in·lb)	6,000	4,000	7,500
Pitching Moment (in·lb)	22,500	7,000	10,000
Yawing Moment (in·lb)	9,750	3,000	4,500

Table 2. Summary of thrust conditions utilized during testing.

C_T	C_T/σ	DL, lb/ft^2
0.004	0.038	4.0
0.006	0.058	6.2
0.008	0.077	8.2
0.009	0.086	9.2

Table 3. Probe rake traverse azimuth, run number and survey schedule for specified rotor height for T613.

Rotor Height		C_T	ψ = 0°		ψ = 180°		ψ = 210°		ψ = 240°		ψ = 270°		ψ = 300°		ψ = 330°	
ft	z/R		Run	Sch.	Run	Sch.	Run	Sch.	Run	Sch.	Run	Sch.	Run	Sch.	Run	Sch.
4.83	0.87	0.006	74	B	97	F					84	B				
					133	G										
		0.009	75	B′	98	F′					85	B′				
					134	G′										
6.32	1.14	0.004	68	A							80	C				
		0.006	69	A′	94	E					81	C′				
					130	G′										
					95	D′					82	D				
		0.008	70	A	131	G	101	D	102	D	88	D^1	103	D	104	D
					142	H					89	D^2				
											105	D^3				
		0.009	71	A′	96	E					83	A′				
					132	G′										
8.31	1.50	0.006			99	E					86	E				
					135	G										
		0.009			100	E′					87	E′				
					136	G′										
9.92	1.79	0.006	72	A	90	E					76	C				
					137	G										
		0.009	73	A′	91	E′					77	C′				
					138	G′										
11.60	2.09	0.006			92	E					78	C				
					139	G										
		0.009			93	E′					79	C′				
					141	G′										

X' is reverse of specified schedule

* probe rake raised: [1] - 1 in; [2] - 2 in; [3] - 2.9 in and inverted

Table 4. Probe rake traverse survey schedule definition.

Traverse Schedule	r/R	0	0.25	0.5	0.55	0.6	0.65	0.7	0.75	0.8	0.85	0.9	0.95	1	1.05	1.1	1.15	1.2	1.25	1.3	1.35	1.4	1.45	1.5
	A																							
	B																							
	C																							
	D																							
	E																							
	F																							
	G																							
	H																							

Traverse Schedule (ctd.)	r/R	1.55	1.6	1.65	1.7	1.75	1.8	1.85	1.9	1.95	2	2.05	2.1	2.15	2.2	2.25	2.3	2.35	2.4	2.45	2.5	2.55	2.6
	A																						
	B																						
	C																						
	D																						
	E																						
	F																						
	G																						
	H																						

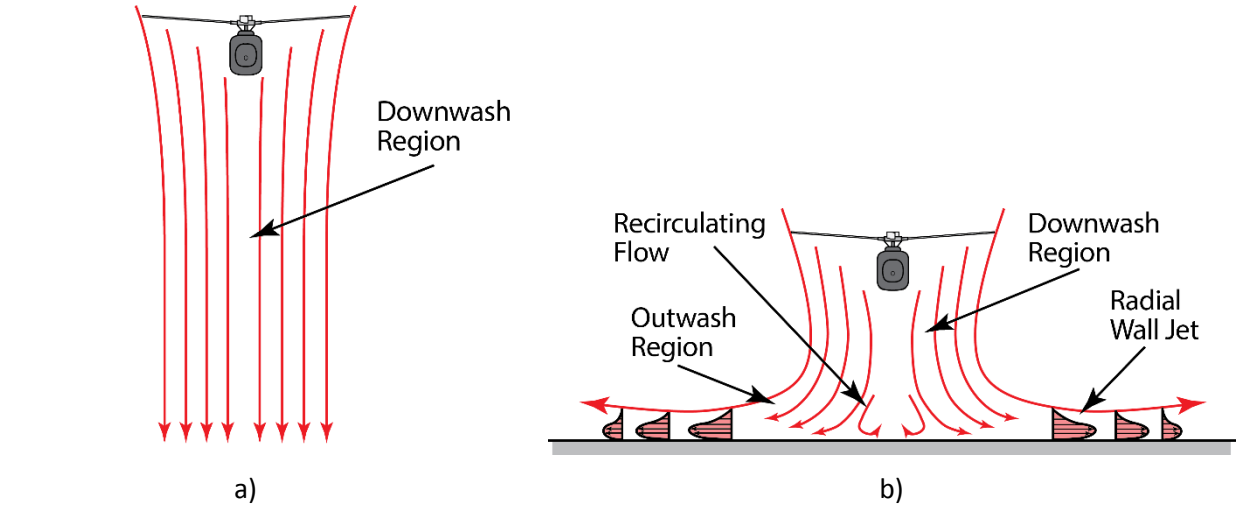

Figure 1. Wake from a hovering rotor: (a) out of ground effect (OGE); (b) in ground effect (IGE).

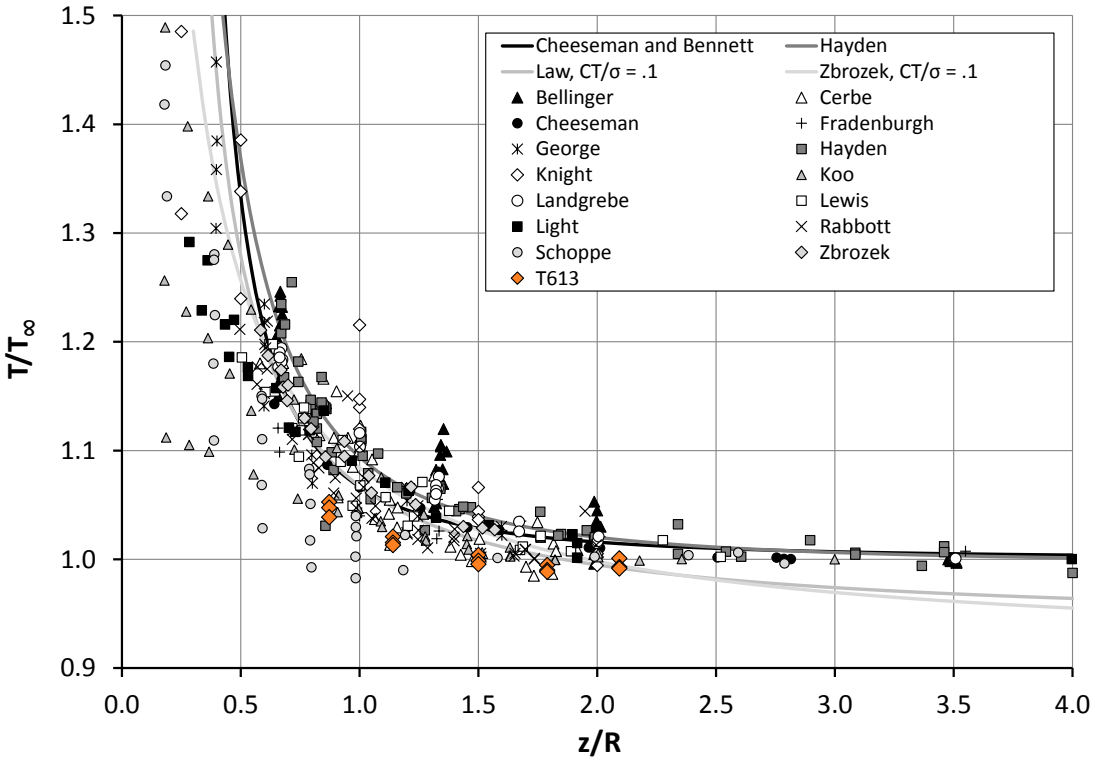

Figure 2. Thrust augmentation versus non-dimensional rotor height; current test data in orange.

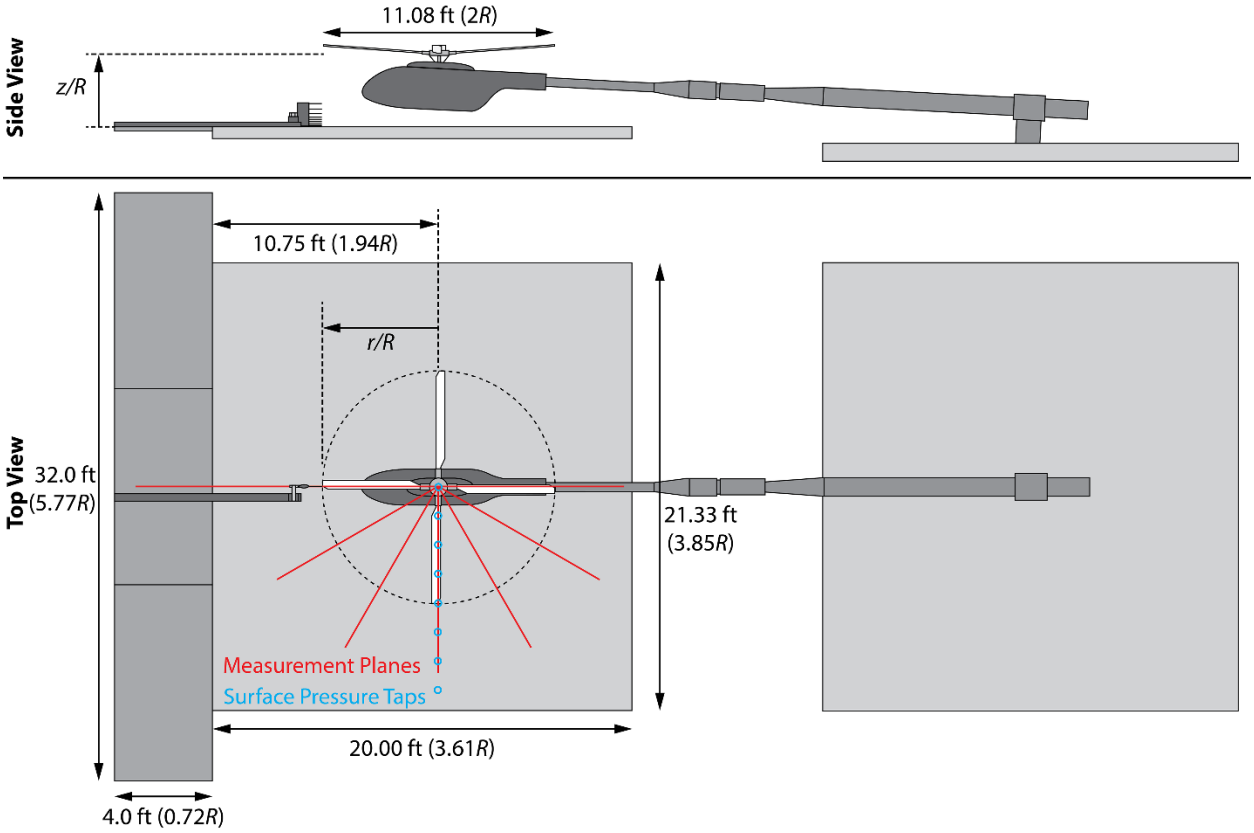

Figure 3. Diagram of T613 setup in RTC during probe rake portion.

Figure 4. GRMS with ROBIN-Mod7 installed in RTC during T613.

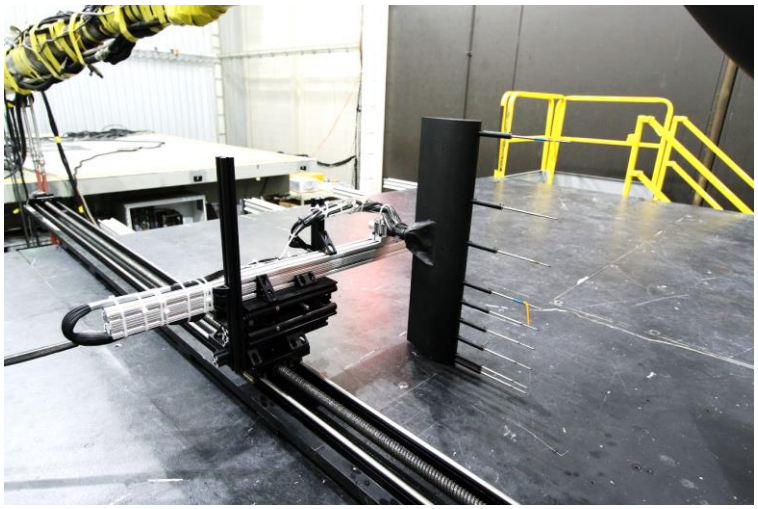

Figure 5. Rake of multi-hole probes installed on remote traverse.

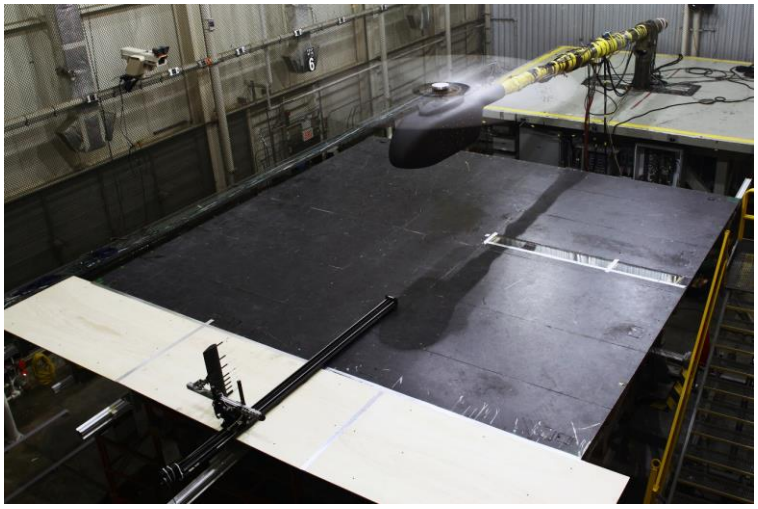

Figure 6. T613 test setup during outwash velocity measurement at z/R = 1.14 with cart extension visible along forward surface and probe rake traverse at ψ = 180° and 2.3 r/R.

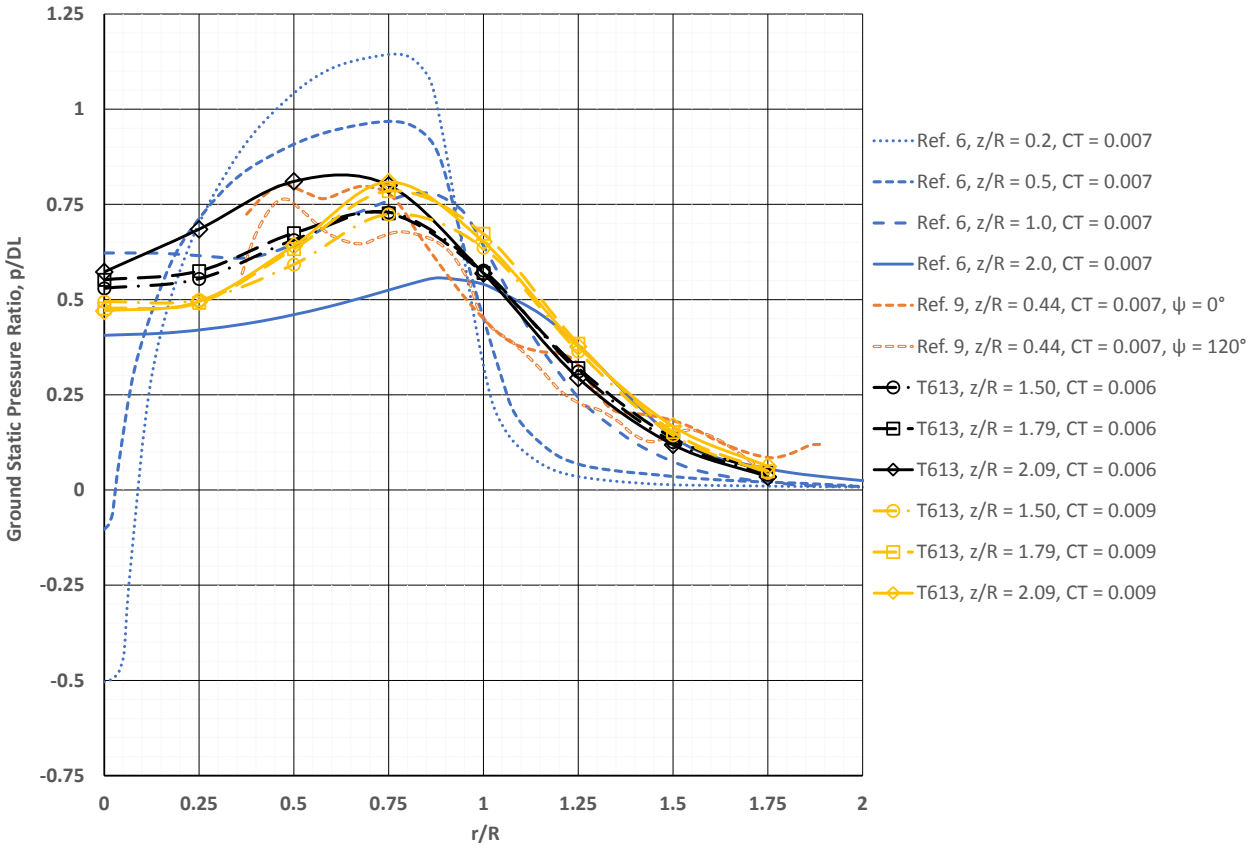

Figure 7. Ground static pressure ratio (*p/DL*) versus radial location *r/R*, historical data from Refs. 6 (blue) and 9 (orange); T613 data obtained at ψ = 270°.

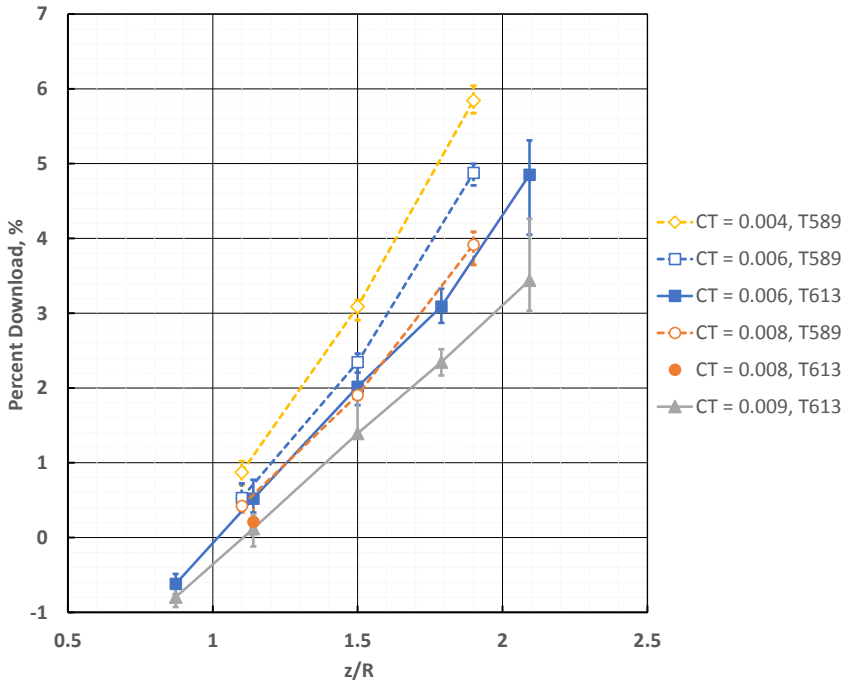

Figure 8. Percent download versus rotor height ratio (*z/R*) for multiple heights and thrust conditions for T589 (dashed) and T613 (solid).

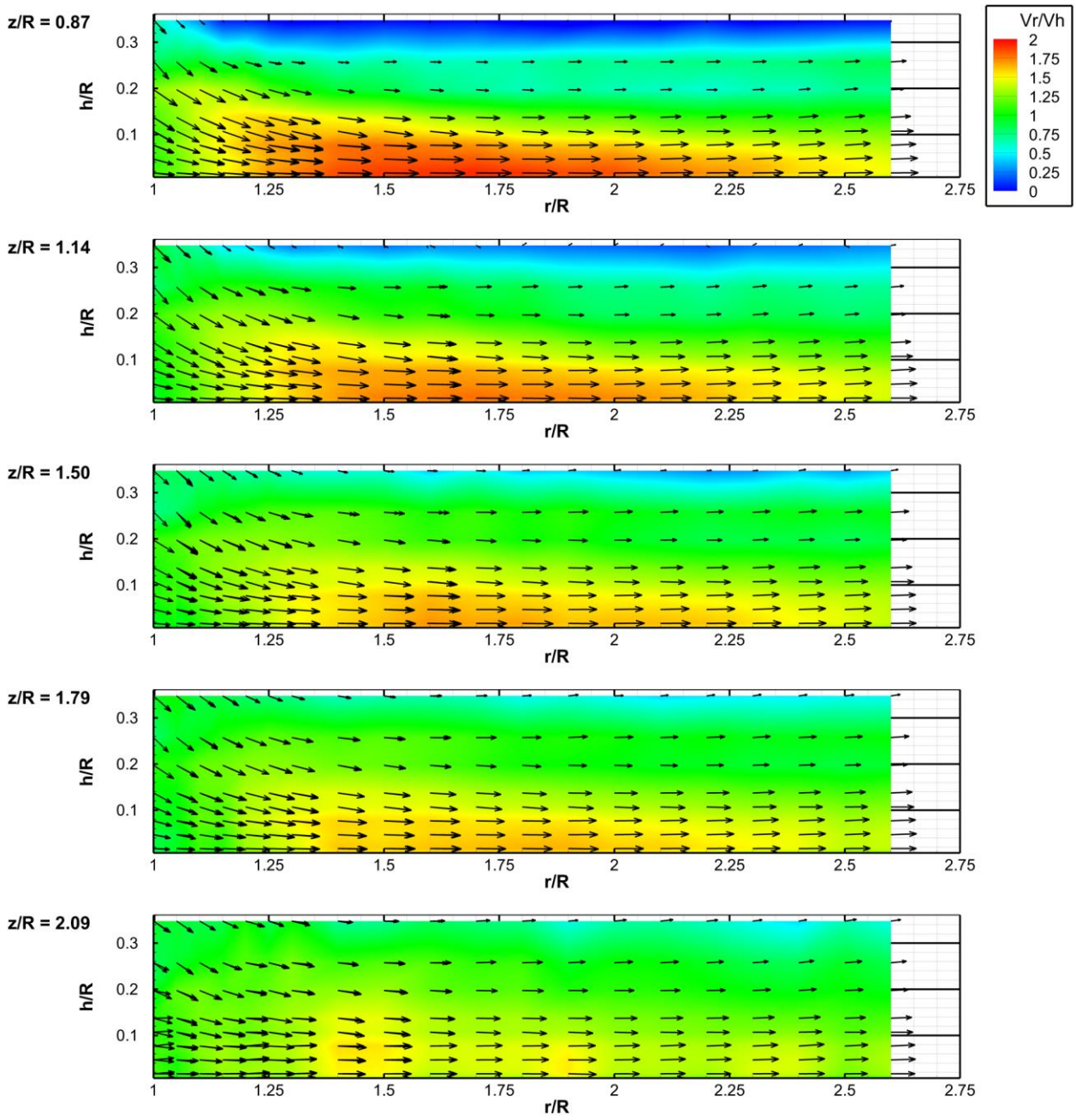

Figure 9. Mean non-dimensionalized outwash velocities and velocity vectors at C_T = 0.008 and ψ = 180° for different rotor heights.

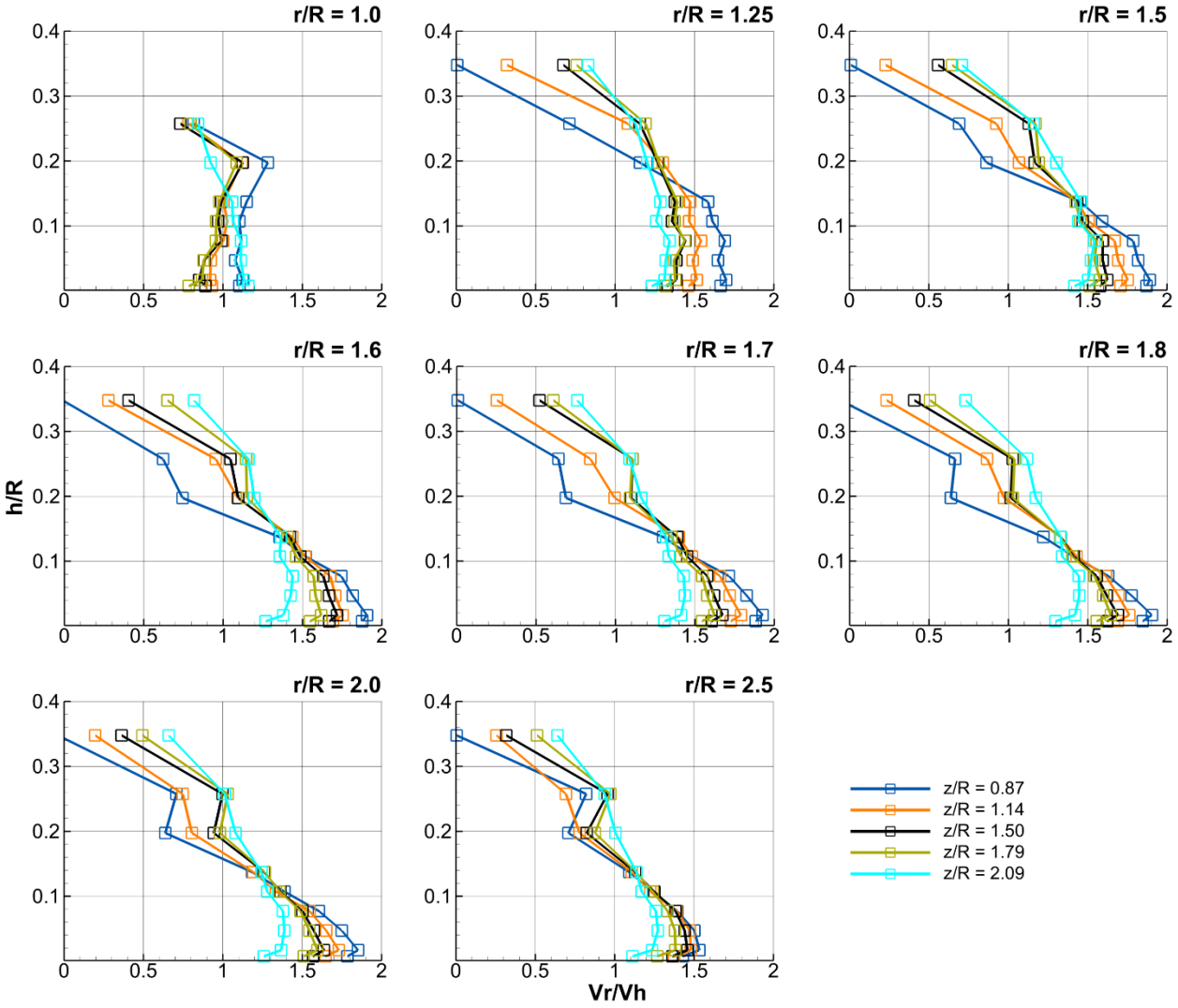

Figure 10. Mean non-dimensionalized outwash velocity profiles at C_T = 0.008 and ψ = 180° at different rotor height ratios for radial station indicated.

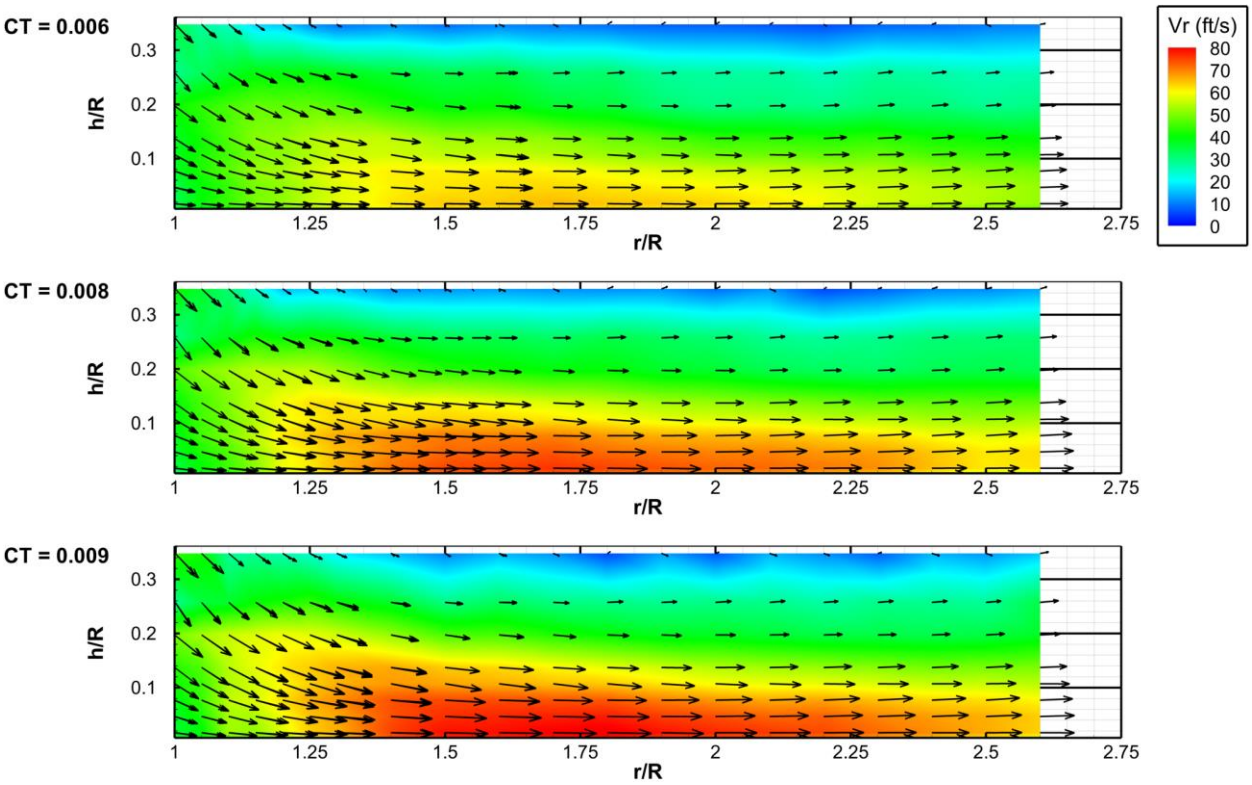

Figure 11. Mean outwash velocities and velocity vectors at z/R = 1.14 and ψ = 180° for different rotor thrust coefficients.

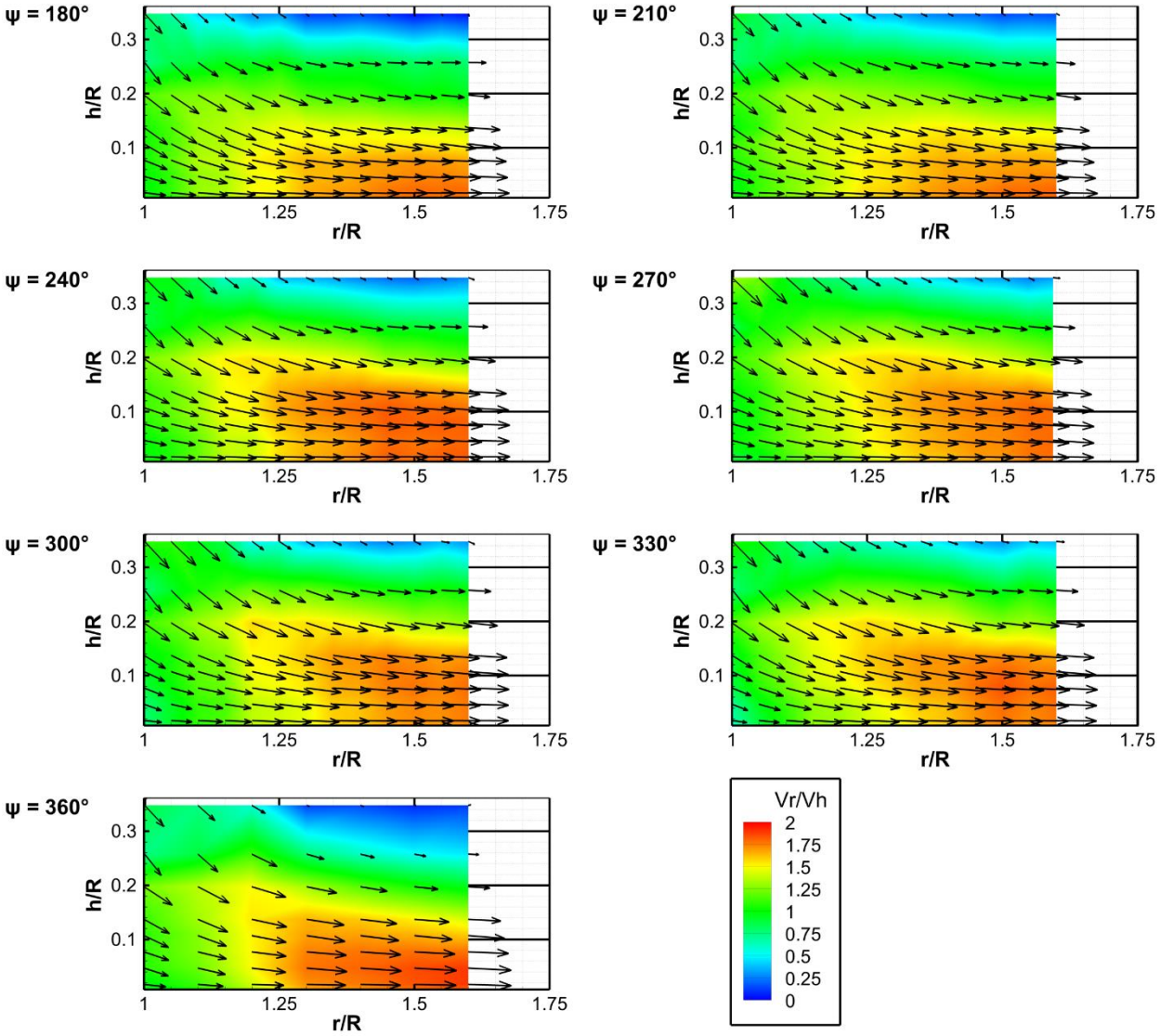

Figure 12. Mean non-dimensionalized outwash velocities and velocity vectors at C_T = 0.008 and z/R = 1.14 at different measurement azimuth locations.

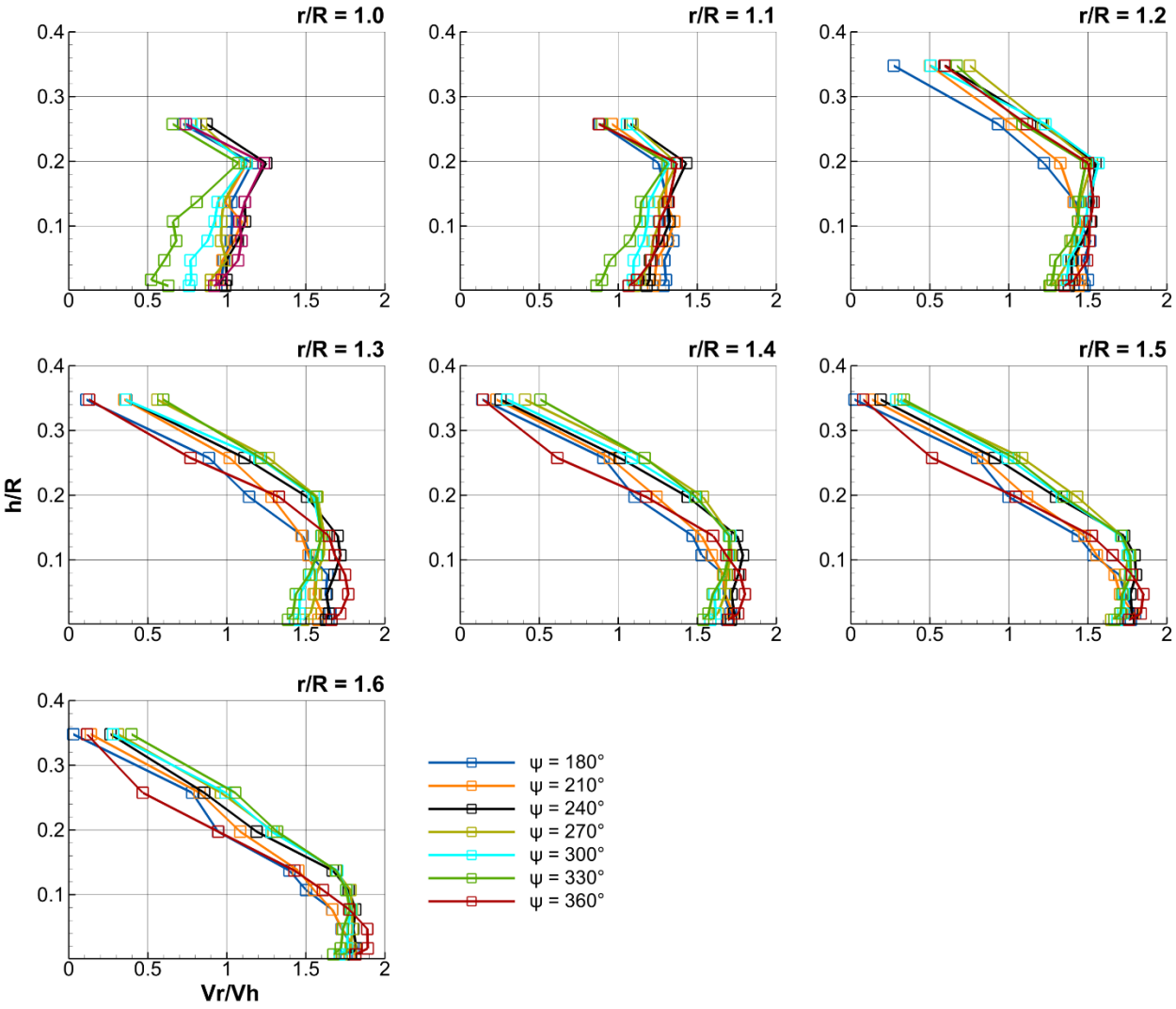

Figure 13. Mean non-dimensionalized outwash velocity profiles with the model at C_T = 0.008 and z/R = 1.14 at different measurement azimuth locations for radial station indicated.

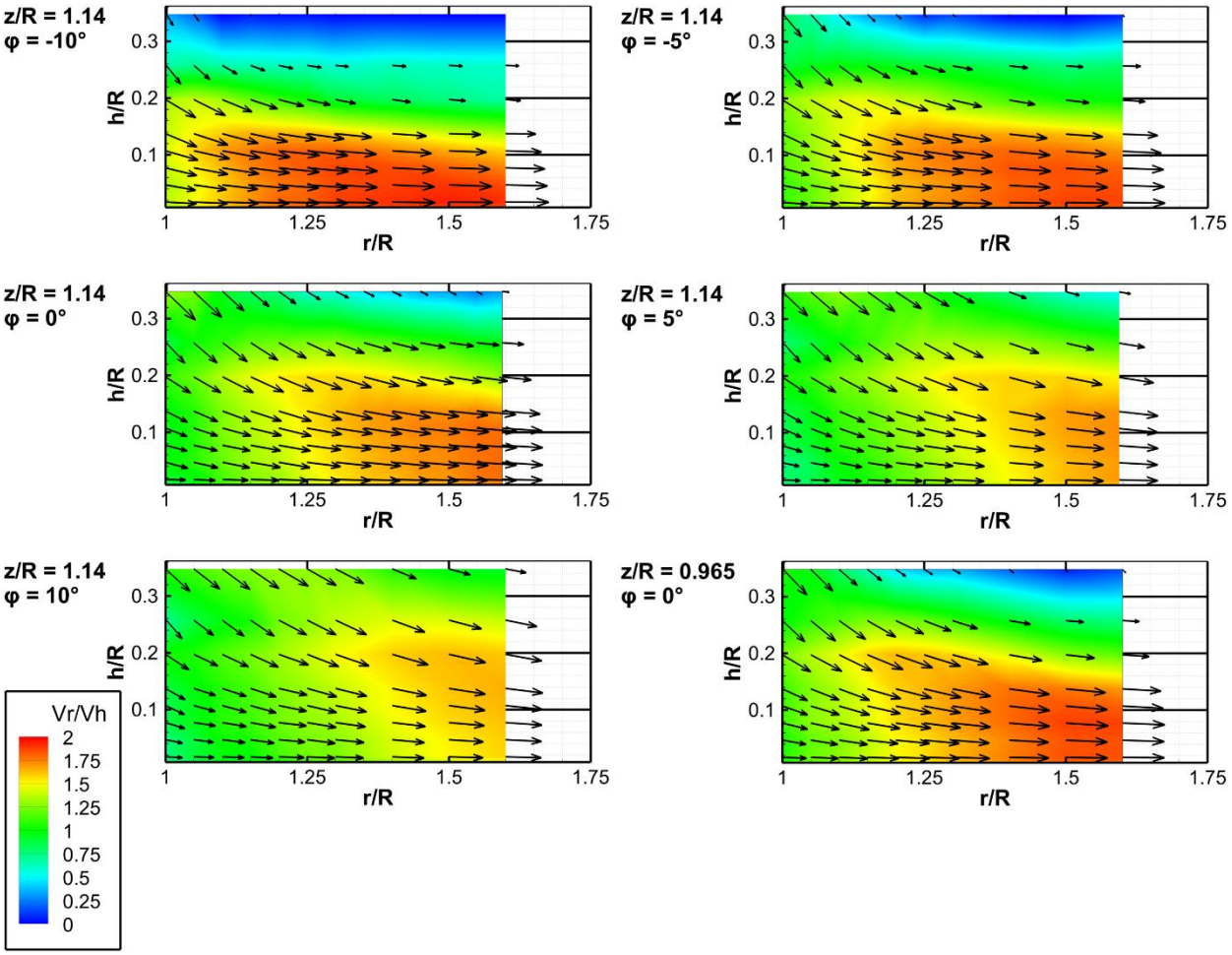

Figure 14. Mean radial non-dimensionalized outwash velocities and velocity vectors at ψ = 270° with the model at C_T = 0.008 and different roll angles and rotor hub heights.

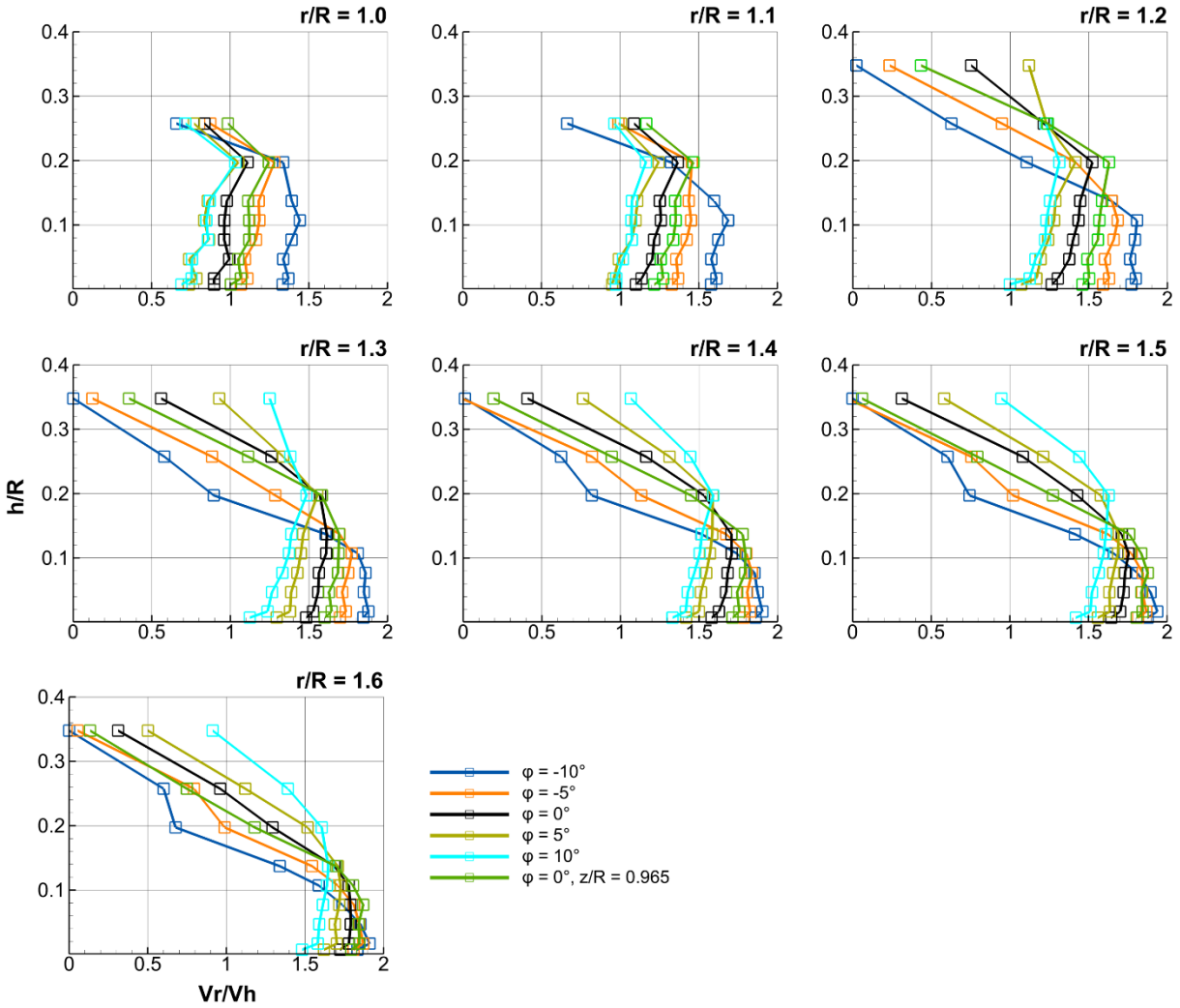

Figure 15. Mean non-dimensionalized outwash velocity profiles at ψ = 270° with the model at C_T = 0.008 and different roll angles and rotor hub heights at radial station indicated.

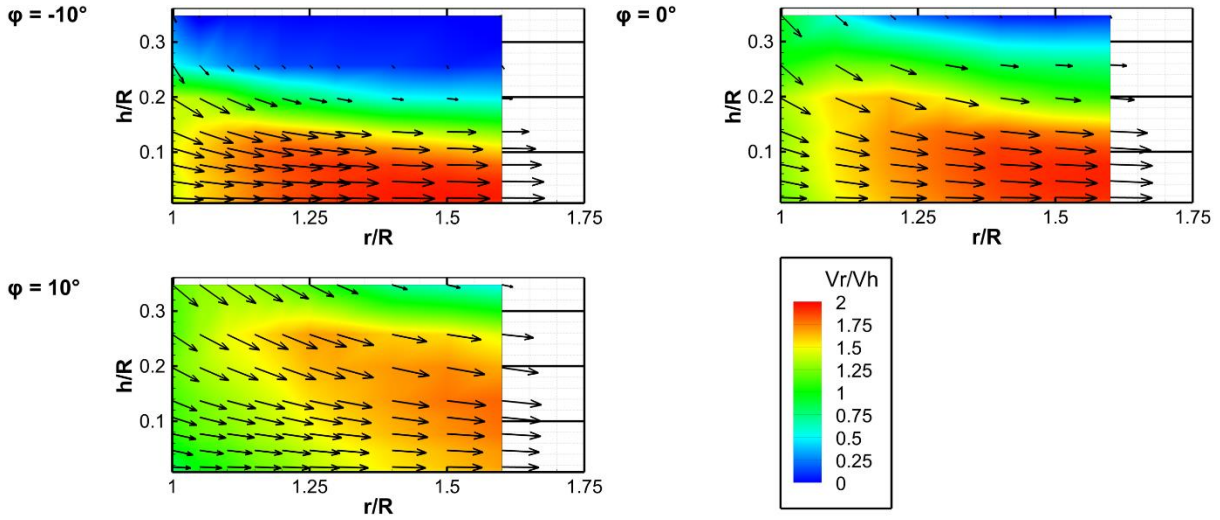

Figure 16. Mean radial non-dimensionalized outwash velocities and velocity vectors at ψ = 270° with the model at C_T = 0.008 and z/R = 0.87 and different roll angles.

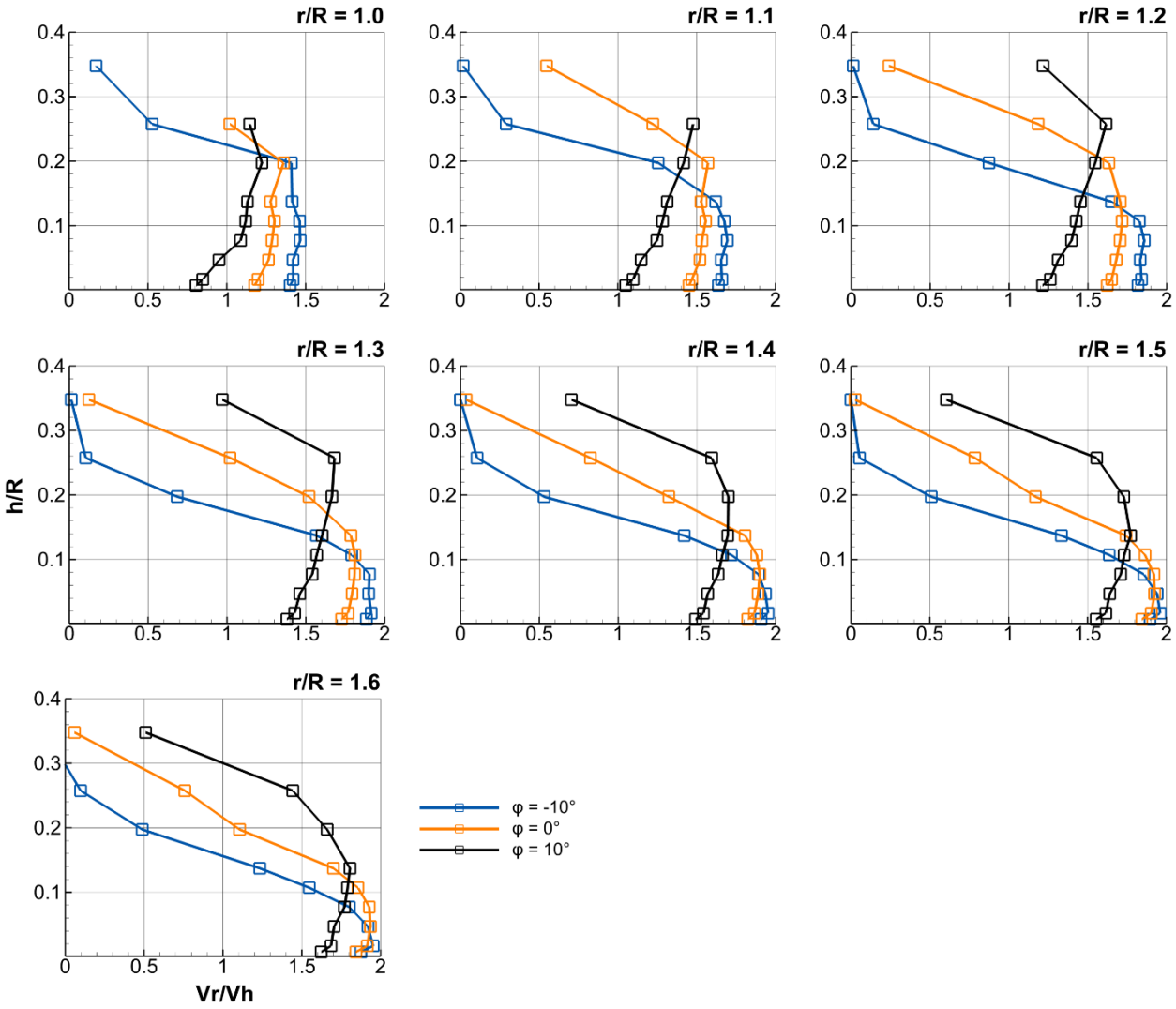

Figure 17. Mean non-dimensionalized outwash velocity profiles at ψ = 270° with the model at C_T = 0.008 and z/R = 0.87 and different model roll angles at radial station indicated.

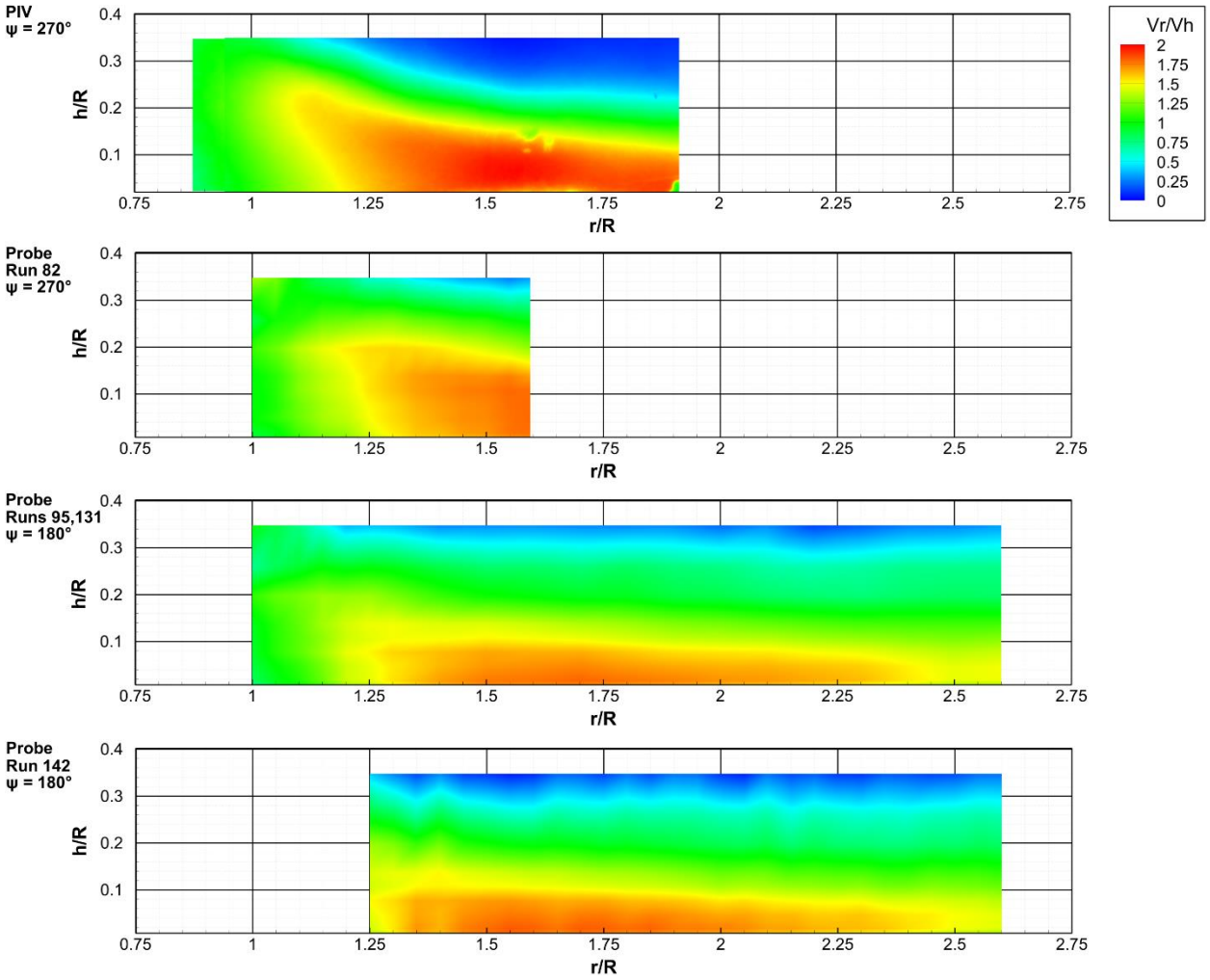

Figure 18. Non-dimensionalized outwash velocities obtained from PIV data from T589 (top) and probe rake data from multiple runs during T613, all at hub z/R = 1.140, C_T = 0.008, and ψ indicated.

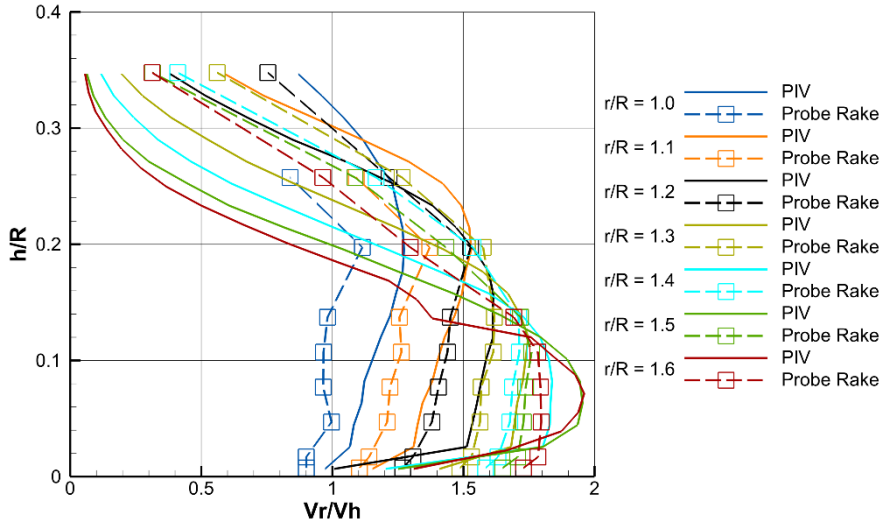

Figure 19. Non-dimensionalized outwash velocity profiles obtained from PIV data from T589 (solid lines) and probe rake data from T613 (dashed lines, from Run 82) at ψ = 270°, C_T = 0.008 and radial station indicated.